The Physics of Ultrahigh-Density Magnetic Recording (Springer Series in Surface Sciences, 41) by M. Plumer (Editor), J. Van Ek (Editor), D. Weller (Editor), G. Ertl (Editor)

Chapter 2

Microstructure of Longitudinal Media

Bin Lu[*] and David E. Laughlin[+]
[*] Seagate Research Center, 2403 Sidney St. #550, Pittsburgh, PA 15203
[+] Materials Science and Engineering Department and Data Storage Systems Center, Carnegie Mellon University, Pittsburgh, PA 15213

2.1 Introduction

In this chapter we give an overview of the effects of various microstructural features on the resulting magnetic properties of magnetic thin films. The role of microstructure on certain properties of materials has a long history of investigation, starting in the discipline of physical metallurgy where the role of microstructure on properties was investigated in great detail [1]. It became clear that some properties were relatively insensitive to changes in microstructure and others were strongly sensitive to changes in microstructure. The former were called *intrinsic properties* or sometimes primary properties, since they were *intrinsic* to the material. The latter were called *extrinsic properties* or secondary properties, since they were dependent on features that were not inherent to the material [2]. With the advent of the discipline of materials science the role of material processing was included in the way extrinsic properties were understood. Changing the method of producing a material often changed some of the resulting physical properties of the material. This change was shown in many cases to be mediated through the change in microstructure of the material. This lead to the so called materials science paradigm: processing determines microstructure which in turn determines the extrinsic properties of a material.

Magnetic thin films are a good example of this paradigm. Small changes in the way a thin film is produced often give rise to large changes in some of the magnetic properties of the thin film. This is best understood by observing how the microstructure of the film changes with processing and then correlating the microstructure directly with the properties of the thin film.

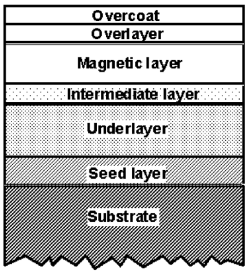

Fig. 2.1 Schematic of the layer structure of thin films used for longitudinal magnetic recording.

A typical structure of a thin film used for magnetic recording is shown in Fig. 2.1. It can be seen that the magnetic layer is in contact with an intermediate layer, which in turn is in contact with an underlayer. The seedlayer and the underlayer set up the grain size as well as the crystallographic orientations in the layers. The intermediate layer enhances the epitaxy growth of the magnetic layer. Furthermore, atoms from the intermediate layer may diffuse up the grain boundaries, giving rise to magnetic isolation of the grains within the magnetic layer. All these processes affect the magnetic properties of the film.

In this chapter we will give an overview of the role that some microstructural features of thin films play in determining the properties of the magnetic layer in films used for longitudinal recording. These features include grain size and grain size distribution, crystallographic orientation, defects and chemical segregation. We will discuss various methods used to control these features during the deposition process and show how with careful control the magnetic properties and hence the recording performance of the films can be optimized.

2.2 The size and distribution of thin film grains

2.2.1 Introduction

High areal density has been achieved in the longitudinal magnetic recording media by continuously shrinking the size of the recorded bits. Since the noise power of magnetic recording media is strongly related to the number of magnetic particles (or grains) per bit, in order to keep the signal to noise ratio (SNR) at a readable level, the number of grains per bit must be maintained above a certain statistical minimum. For this reason the average grain size in the magnetic layer has been scaled continuously with the bit length and the track width. This can not continue indefinitely, as the magnetic energy stored in each grain (K_uV) is becoming so small that the thermal energy (k_BT) is approaching the same magnitude. When this happens the superparamagnetic limit is reached and the media is no longer thermally stable [3] (also see Chapter 5).

Therefore the effect of grain size is two-fold. On the one hand the grains should be small enough to keep high SNR, on the other hand the grain size should be large enough to keep the recorded information thermally stable. For Co-alloy media, assuming a $K_u = 2.5 \times 10^6$ erg/cc, and a cubic grain shape, and using the media stability criterion of $K_uV/k_BT \geq 60$ (thermally stable for 10 years) [3], the smallest grain size that can be used at room temperature (300K) is calculated to be about 9.7 nm. In fact, in the 10Gbits/in^2 media design announced in 1998 [4], the grain size was about $D = 12 \pm 4$ nm. It is obviously that there is little room left for grain size reduction with the current Co-alloy media.

Another important feature is grain size distribution. The sizes of the grains in media are not uniform but are spread about an average value. The information stored in the smaller grains decay more rapidly, while the larger grains give rise to a higher noise level. It has been reported by Weller and Moser [5] that narrowing the grain size distribution can alleviate about 25% of the thermal decay problem. Likewise, it will also significantly enhance the signal to noise ratio (SNR).

When discussing grain size and grain size distribution, it is usually assumed that the Co-alloy grains are magnetically well separated by nonmagnetic grain boundaries, which either consist of nonmagnetic materials or simply voids. If this assumption is not true, magnetic clusters of grains must be taken into account [6,7]. These magnetic clusters consist of several grains magnetically coupled by inter-granular exchange coupling. The grains inside a magnetic cluster behave in concert under magnetic fields. Therefore for media with strong exchange coupling, the effective magnetic particle size will be much larger than the grain size, causing a higher media noise [8-12]. On the other hand, there is also a possibility of forming microstructural clusters, inside which the grains are of similar crystallographic orientation. The grain boundaries inside such clusters are less distinguishable than the cluster boundaries. In such a case, the media noise depends strongly on the microstructural cluster size [13].

For these reasons the control of the grain size and grain size distribution of the underlayer and magnetic layer is of critical importance to control and to optimize the magnetic properties and recording performance of the magnetic media.

2.2.2 Grain size distribution

Three kinds of distributions can be used to describe grain size distribution.

1. Gaussion (Normal) distribution:

$$y = \frac{1}{\sigma\sqrt{2\pi}} \exp\left(-\frac{(x-A)^2}{2\sigma^2}\right) \tag{2.1}$$

where, A is the arithmetic mean and σ is the standard deviation.

2. Log normal distribution:

$$y = \frac{1}{\log\sigma_g \sqrt{2\pi}} \exp\left[-\frac{(\log x - \log x_g)^2}{2\log^2 \sigma_g}\right] \tag{2.2}$$

It can be seen that the log normal distribution is formed from normal distribution by substituting log$x$ in equation (2.2) for x. As a result, x_g is the geometric mean,

and σ_g the geometric standard deviation, whose logarithm is the standard deviation of the variable log *x*.

3. Rosin-Rammler Distribution:

$$y = \frac{n}{d^n} x^{(n-1)} \exp(-\frac{x^n}{d^n}) \text{ , (n > 1)} \quad (2.3)$$

The parameter *n* primarily depends on the skew of the distribution and the parameter *d* is primarily determined by the breadth of the distribution.

Since the Rosin-Rammlar distribution has two parameters, it can be easily fit to the grain size distribution in Co-alloy films [14]. However, both the normal and Rosin-Rammlar distribution allow for negative variable values, which are not physically applicable to grain size distributions.

The log normal distribution allows only positive variable values. Moreover, it has been found by Soderlund *et al*. [15] that in thin film deposition, if the adatoms diffuse or drift within a small but finite region, the time of growth of the nuclei before impingement can be accurately described by a log normal distribution. This will cause the grain size distribution to be a log normal one. It has been shown that the grain size distributions of CoCrPt, CoCrPtTa and CoCrPtB alloy thin films are log normal [16]. Hence, many calculations of magnetic properties of the media use the log normal grain size distribution [5].

It should be noted that when we consider the signal read from each recorded bit, it is the grain area distribution by area fraction that should be counted rather than the grain area distribution by count fraction. This is because the signal contributed by an individual grain is proportional to its moment, $M_r tS$, where M_r is the remnant magnetization of the magnetic layer and *t* is the layer thickness. Due to columnar growth of the grains, $M_r t$ is constant through out the entire media, the distribution of the signal from each grain should be expressed as grain area distribution by area fraction. Fig. 2.2 shows the difference between the grain area distribution by count fraction and by area fraction for CoCrPt media.

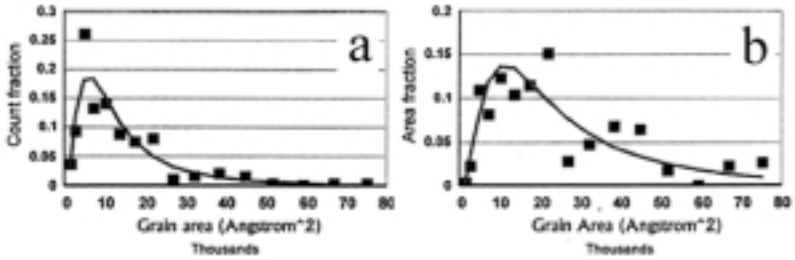

Fig. 2.2 Grain size distribution by number and by area in a longitudinal media [17] (© 2000 IEEE).

At the initial nucleation stage of film deposition, a minimum number of atoms are required to form a critical nucleus. A sub-critical nucleus is unstable and will dissolve. Critical nuclei are small. For example, the size of critical nuclei for Zn on glass at room temperature (RT) is about 0.3 nm [18], it is 1.2 nm for Mg [18] on glass at RT, 1-2 nm for Cr on NiP [19], 3-5 nm for CoCrTa on Cr at 250°C [20]. Since the grains cannot be smaller than the critical nucleus, there is a characteristic truncation on the left-hand side of the grain size distribution.

Therefore, when the mean grain size approaches the size of the critical nucleus, the grain size distribution will tend to be narrower. Based on this reasoning, most of the current research focuses only on how to reduce the average grain size, expecting a corresponding decrease in the distribution breadth [17].

2.2.3 Control of grain size

In longitudinal media the Co-alloy grains are epitaxially grown on underlayers or intermediate layers, mostly consisting of Cr-alloy films, while adatoms of the Cr-alloy (CrX) films nucleate randomly and grow on the smooth surface of amorphous NiP or glass. Therefore, the control of the grain size and grain size distribution of the magnetic layer is realized through controlling the nucleation and growth of the CrX underlayer on the substrate.

The initial grain structure is formed following models of nucleation and growth-to-impingement. The heterogeneous nucleation of CrX on a smooth amorphous substrate can be described by capillarity theory [21]. According to the theory the nucleation rate is a strong function of the nucleation critical energy ΔG^*, which is the critical free energy of forming the nuclei. ΔG^* varies with deposition rate, substrate temperature, surface roughness and other factors.

Generally, ΔG^* increases with substrate temperature and decreases with deposition rate [22]. Consequently, the number of stable nucleus decreases rapidly with substrate temperature increase and a continuous film will take longer to develop, which results in larger grains. On the other hand, a larger number of stable nuclei form at higher deposition rates, and a continuous film is produced at lower average film thickness with smaller grain size.

After impingement, the growth of the grains is also affected by deposition conditions, such as, substrate temperature, the sputtering power, the argon pressure, etc. Thornton's zone model [23-25] best classifies the final morphology of the sputter deposited metal films. Fig. 2.3 shows the morphology of the film varying with the Ar pressure and substrate temperature. According to this model, at low temperatures ($T_{sub}/T_m<0.3$, where T_{sub} is the substrate temperature and T_m is melting point of the material) and high Ar pressure, the film consists of tapered crystals with domed tops which are separated by voided boundaries. The internal structure is poorly defined, with a high dislocation density. The grain size increases with T_{sub}/T_m. The morphology of the films falls into Zone 1 of the model. This kind of deposition condition used to be utilized to grow very thick underlayers in order to enhance the voided grains boundaries, which decouple the magnetic grains and consequently give rise to lower media noise [26-31].

At higher substrate temperatures ($0.3 < T/T_m < 0.5$) and lower Ar pressures, the films consist of columnar grains separated by distinct dense grain boundaries. These grains are highly faceted at the surface of the films. Dislocations are primarily in the boundary regions. The nucleation energy is about equal to that for surface diffusion. This is defined as Zone 2. Zone T is a transition zone with processing parameters between those of Zones 1 and 2. A film in Zone T consists of a dense array of poorly defined fibrous grains without voided boundaries. The columnar grain diameter also increases with T_{sub}/T_m.

The influence of the substrate temperature, Ar pressure and substrate roughness has been discussed in detail in Thornton's review paper [23]. Further description of both thick and thin films has been reported by Grovenor *et al.* [25]

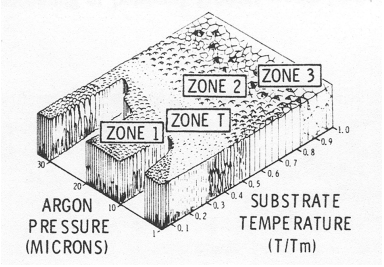

Fig. **2.3** Thornton's Zone model for sputter deposited metal films [23] (with permission, from the *Annual Review of Materials Science*, Volume 7 © 1997 by Annual Reviews www.AnnualReviews.org).

DC magnetron sputtering deposition at moderate substrate temperatures (300K- 550K) is normally used in the manufacturing of magnetic recording media. The deposition rate is very high in the process (about 1000nm/min). From the start, the nucleation rate is high but quickly decreases to zero as the number of nuclei saturates on the substrate. The substrate temperature for the Cr layer (T_{sub}/Tm) is about 0.14 - 0.25 and the Ar pressure is about 3 –10 mtorr. For room temperature deposition of Cr (110) films, many defects and voids have been observed [29]. In this case the nucleation and growth conditions belong to Zone 1 of the Thornton's model. For Cr (200) textured layers deposited at 250°C, the deposition condition is in Zone T. Therefore, well defined columnar grains are commonly observed in the CrX thin films.

Columnar growth is primarily controlled by the competition between discrete atomic deposition and surface diffusion [32]. Assuming no coalescence, the average grain diameter, D, is related to the grain growth rate, G, and the nucleation rate, I, by [33]

$$D = 1.448 \times (\frac{G}{I})^{\frac{2}{3}} \qquad (2.4)$$

Therefore, any conditions which affect the nucleation or growth rates have a corresponding influence on the grain size. Many methods of grain size control have been studied based on the above theories. Depending on the layer structure of a media, those methods can be classified into the following categories: a) substrate surface modification, b) seedlayer studies, c) underlayer studies.

a) Surface modification of the substrate has not been considered as a method for grain size reduction until recently. Lightly oxidized NiP or NiP-Co plated Al-Mg substrates can be used to prepare smaller Cr grains [34]. Table 2.1 shows that exposing the substrate to oxygen after dry etching helps to reduce the Cr grain size and also narrows its distribution (σ is the standard deviation).

Table 2.1 Dependence of grain size on O_2 exposure [34] (© 2000 IEEE).

Media	O_2 (L)	Grain size (nm)	σ (nm)
A	0	10.8	3.9
B	1.5	9.8	3.3
C	3.5	9.3	2.9

Table 2.2 Dependence of grain size on Co concentration in Co-NiP coating [34] (© 2000 IEEE).

Media	Co (ppm)	Grain size (nm)	σ (nm)

B	0	9.8	3.3
E	120	9.6	3.1
F	400	8.8	2.9
G	1200	8.6	2.7

When Co is added to the NiP coating and oxidized, it is believed that Cr (5nm thick) nucleates much easier at the Ni-O or Co-O sites than on NiP substrate without oxidation. Therefore, the nucleation rate will be high and the grain size will be smaller. Table 2.2 shows that the average grain size and the standard deviation of the distribution can be reduced by this method.

Surface roughness is also one of the factors that affects the nucleation rate by affecting the wetting factor of the critical nucleation energy. Chang *et al.* [19] have demonstrated that the nano-roughness of the seedlayer will vary the wetting of the Cr nuclei, increasing the nucleation rate of the Cr film, thus, decreasing the grain size of the Cr layer. Using HRTEM, the authors also found fewer nuclei with size of 2-3 nm on the smooth NiP layer, while the nuclei were 1-2 nm on surface treated NiP layer (with nano-roughness). The smaller nuclei are speculated to be due to the rougher surface and to be located in the valleys of the rough NiP layer. As the Cr layer gets thicker (10 nm), the Cr grains on smoother NiP layers coalesce into larger grains with size of 30nm, while the Cr grains on the nano-rougher NiP layers maintain their orientation and particle coalescence does not occur. This results in a smaller Cr grain size and a more uniform distribution.

b) Seedlayer is another important factor in controlling the grain size. Matsuda *et al.* [35] have found that a seedlayer of oxidized CoCrZr not only enhances the CrTi (200) texture but also reduces the grain size. The authors believed that Zr was selectively oxidized. As a result, ZrO nucleation sites can be formed at the seedlayer surface controlling the nucleation rate and growth of the subsequent CrTi layer. Likewise, the use of Ta_2O_5 [36] or NiP [37] seedlayers has also been reported to reduce the media grain size.

c) The underlayer is the layer that has been extensively studied in controlling the grain size of magnetic layer. The gain size of the NiAl underlayers are reported to be smaller than that of the Cr [38]. This is due to the stronger intermetallic bonds between the Ni and Al atoms than between the Cr bonds, which results in smaller nucleation energy and less diffusion. Therefore NiAl films have a higher nucleation rate and subsequently smaller grain size [39].

The grain size of the underlayer can also be controlled by it own thickness. However, if the underlayer (CrX) is too thin (less than 10 nm), the film does not have a strong crystallographic texture. This will result in poor orientation and an increase of defect density in the magnetic layer. It is commonly observed that H_c increases with Cr thickness and levels off after a certain thickness [30]. To overcome this problem, ultra clean (UC) processes were adopted to obtain good microstructural and magnetic properties with thinner Cr underlayer thickness and lower M_rt of the magnetic layer [40][41]. The reason for the effect of the UC process is not clear, but removal of oxygen, water vapor and nitrogen in the sputtering chamber is helpful in obtaining better surface mobility of the adatoms and less defects, during both the Cr and Co-alloy deposition.

Choosing alloys with higher melting temperatures, like CrW [42], to reduce T_{sub}/T_m is another practical way of decreasing the grain size. Moreover, the underlayer composition also affects the nucleation rate and growth kinetics, which eventually affects the grain size. Hosoe *et al.* [43] reported that CrTiB has a larger grain size (11 nm) than that of CrTi (9.5nm) when DC magnetron sputter deposited onto NiP-plated Al-Mg substrates.

Table 2.3. Dependence of grain size on underlayers [45] (© 1999 IEEE).

Seedlayer	underlayer	<d> (nm)	σ/<d>
Ta/Zr	CrTi	15.9	0.31
	CrTiB	10.5	0.27
CoCrZr	CrTi	9.1	0.24
	CrTiB	7.1	0.18

The same group has shown that a CoCrZr seedlayer has an effective influence on grain size reduction of the CrTi underlayer [44]. By combining the CoCrZr seedlayer and CrTiB underlayer the authors obtained the grain size reduction. Table 2.3 shows that the underlayer grain size is significantly influenced by boron additions and the type of seedlayer. The smallest grain size is 7.1 nm. The table also shows that when the average grain size of the underlayer is reduced, the dispersion of the grain size distribution is reduced as well.

In summary, the grain size of the magnetic Co-alloy thin films can be controlled through modifications of the substrate, the seedlayer and the underlayer. However, there is currently no known method to narrow the grain size distribution other than reducing the average grain size and expecting that the log normal distribution will narrow itself accordingly. To significantly narrow the grain size distribution, regular arrays of nucleation sites must be prepared on the substrate or seedlayer. There are ways of producing mono-dispersed magnetic particles by chemical synthesis [46,47] (also see Chapter 9); however, this method has not yet been implemented in the production of recording media.

2.3 Crystallographic orientation

2.3.1 Introduction

For materials with the hcp structure a common texture is (00.1) when sputter deposited onto an amorphous substrate, i.e. the (00.1) planes are parallel to the plane of the film. In this case, there is often a mixture of hcp and fcc phases present, which causes poor magnetic properties for magnetic recording [48]. To make the c-axis of Co-alloy grain lie in or close to the film plane for use as longitudinal media, underlayers must be sputtered before the Co-alloy layer. It has been nearly a quarter of century since the discovery of bcc Cr underlayers [49,50]. Due to the similar atomic size of Cr and Co, there are several possible orientation relationships between the bcc Cr grains and the hcp Co grains. Three relationships that have been used in longitudinal media are shown in Fig. 2.4.

It can be seen that Co (10.0) and Cr (112) planes have the best lattice match. Actually the ratio of the two sides of the Cr (112) lattice plane is $\sqrt{8/3}$, which is

exactly same as that of the Co (10.0) plane. For this reason, a perfect lattice match can be realized between Co-alloy (10.0) plane and a Cr-alloy (112) plane by varying the composition of the Cr-alloy.

When the Co thin film is oriented in a (10.1) texture, its c-axes are about 28.1° away from the thin film plane, while in the (11.0) and (10.0) texture, the c-axes are in the film plane. Much research has been performed to make single crystal Co-alloy thin films with these three kinds of orientations, not only to demonstrate the lattice matching but also to obtain the intrinsic magnetic properties (such as the magnetocrystalline anisotropy) of Co-alloy thin films. When Ag/Si templates are used, the epitaxial relationships between the substrate and thin films are:

Co(10.1)/Cr(110)/Ag(111)/Si (111) [52]
Co(11.0)/Cr(200)/Ag(200)/Si (200) [53,54]
Co(10.0)/Cr(112)/Ag(110)/Si (110) [55]

When MgO single crystal substrate is used the epitaxial relationships between the substrate and thin films are:

Co-alloy (11.0)/Cr (200)/MgO (200) [56,57]
Co-alloy (10.0)/Cr (112)/MgO (110) [58]

Other single crystal substrates such as, Cr (100) and Cr(110) [59], GaAs (100) [60], LiF and NaCl (100) [61] have also been studied. Reviews of the growth of single crystal Co-alloy thin films and their basic magnetic properties can be found in Ref. [62] and [63].

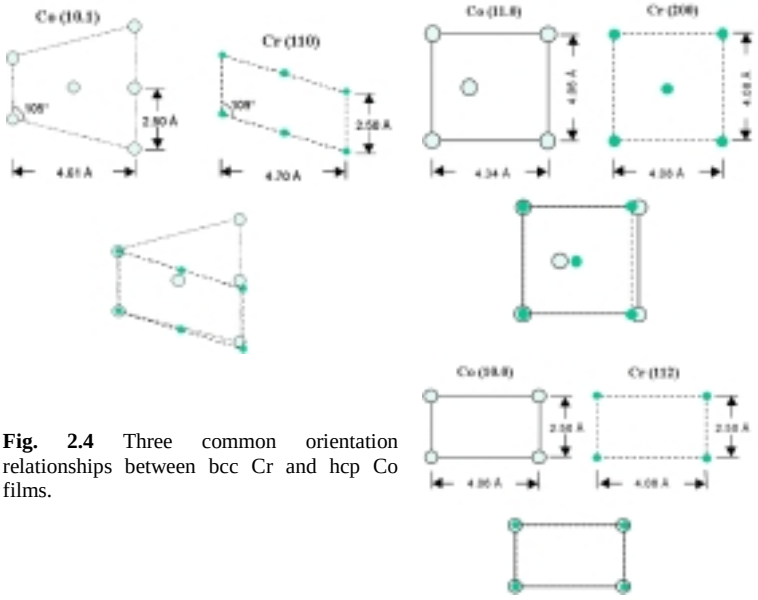

Fig. 2.4 Three common orientation relationships between bcc Cr and hcp Co films.

It is not practical to use single crystalline thin films for longitudinal magnetic recording, because the angular variation of H_c, M_rt and S* in different circumferential directions will cause a modulation of output signals. Therefore it is better to allow the Co-alloy films to have their c-axes randomly oriented in the film plane. From the results of epitaxial growth of single crystal films, one can see

that the availability of the (10.1), (11.0) and (10.0) textured Co-alloy thin films depends on the availability of the Cr (110), Cr (200) and Cr (112) textured underlayers, respectively. Reviews on the control of the texture orientation of polycrystalline Co-alloy thin films for longitudinal magnetic recording can be found in Ref. [51] and [64]. A detailed electron diffraction study of polycrystalline Co/Cr bilayers can be found in Ref. [65] where some of the less frequently occurring orientation relationships, such as Co (11.0)/Cr (111) and Co(10.0)/Cr (113) were also observed by electron micro-diffraction.

When Cr is deposited onto an amorphous substrate at room temperature, it yields films with (110) texture. Early longitudinal magnetic recording media had Co-alloy grains either randomly oriented [66] or with (10.1) preferred orientation [67]. Consequently the magnetic easy axis (c-axis) of the grains were either 3D randomly oriented or were oriented 28.1° from the film surface. In the latter case, the Co (00.2) texture can also be developed because there is certain degree of lattice matching between the plane Co (00.2) and Cr (110). As a result, there is a good portion of Co-alloy grains oriented with their c-axes perpendicular to the film, which is undesirable for the longitudinal recording. Therefore, the media with Co (10.1) texture were replaced by ones with the Co (11.0) texture.

Several research groups discovered in the late-1980's that films with Cr (200) texture could be grown when the films were deposited at elevated temperatures [68-70]. This texture of the underlayer lead to Co-alloy films with (11.0) texture, as shown by Daval and Randet [71] in 1970. For (11.0) textured Co-alloy films, the c axes are 2D-randomly oriented in the film plane. Moreover, when combined with circumferential mechanical texturing the films can give rise to in-plane circumferential anisotropy [72,73], that renders excellent recording properties [74,75]. However, the roughness introduced by mechanical texturing [76] increases the head to disk spacing. High-density recording requires that the heads fly as close to the media as possible. Hence there is a trade off between obtaining a smooth media surface and obtaining circumferential anisotropy. On the other hand, glass substrates not only have smoother surfaces but also have mechanical advantages over NiP/Al-Mg substrates. High recording density media on glass substrates was made possible [4] after the introduction of the NiAl (112) underlayer as described below.

A distinctive feature of media with the Co-alloy (11.0) on the Cr (200) texture is its bicrystal structure [77,78]. Since the c-axis of Co-alloys can align with either of the <110> directions in the Cr (200) planes, the Co-alloy can form bicrystals with c-axis 90° to each other (Fig. 2.5).

The advantage of bicrystal grains is that they refine the grain size of the media and may reduce recording noise [79,80]. The disadvantage is that they are very likely to be exchange coupled with each other. The compositional studies have shown that Cr segregation at the bicrystal grain boundaries is much less than that at the regular grain boundaries [81]. This indicates that Cr segregation at the bicrystal boundaries is not sufficient to magnetically decouple the grains. When two bicrystals are exchange coupled, the diagonal directions between the orthogonal oriented c-axes are effectively easy axes, while either of the c-axes directions becomes effective hard axes [82]. In this case, the anisotropy energy (K_u) of an exchange coupled bicrystal grain is significantly decreased [83].

Obviously, the chances of having several bicrystals nucleate on one underlayer grain decrease with the decrease of underlayer grain size, viz. there will be a small amount of bicrystals in high density recording media with smaller grain size.

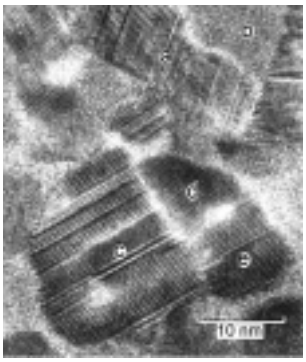

Fig. 2.5 Bicrystals of a CoCrTa film on Cr underlayer [77] (© 1995 IEEE, courtesy of Y. Hosoe).

Co-alloy (10.0) on Cr (112) are the most desirable textures for longitudinal media. Theoretically it can have a perfect lattice match. It does not produce bicrystals. However, due to its higher Miller indices, the (112) textured Cr films are very hard to obtain. In 1994 Lee, *et al*. [38] reported that NiAl can develop (112) texture when deposited onto amorphous substrates. NiAl has B2 (CsCl) structure, which is a bcc derivative structure. It also has nearly the same lattice parameter as Cr. Therefore, Co (10.0) textured film can be obtained when deposited either directly onto NiAl or on a Cr (112) intermediate layer. The magnetic properties of Co(10.0)/NiAl(112) films are inferior to the bicrystal Co(11.0)/Cr(200) media. However, once a thin Cr intermediate layer is added the magnetic properties improve greatly, exceeding the (11.0) oriented media [84].

It was later found and suggested by Lu *et al*. that the function of Cr intermediate is two-fold. First it inherits and continues to enhance the (112) texture epitaxial growth [85]. Secondly, it has metallic bonds, which are non-directional, compared to NiAl, whose bond types are a mixture of metallic, ionic and covalent with directional character [86,87]. The Co-alloy has hcp structure, which is different from the cubic B2 structure of NiAl, the directional bonds of NiAl make it difficult for the Co-alloy to epitaxially grow on it. Adding a layer of Cr enhances the epitaxy between the hcp Co alloy and its underlayer [88].

The weaker (112) texture of NiAl causes the Co-alloy (10.0) texture to be weaker than the Co-alloy (11.0). Thus, a portion of the Co-alloy grains are randomly oriented [85]. In this case, fcc regions and stacking faults cannot be controlled by the Cr to Co-alloy epitaxy. As a result, the randomly oriented grains not only have undesirable c-axis orientation but also have lower anisotropy energy. On the other hand, the epitaxially grown grains have perfect lattice match with the underlayers. These grains contain less stacking faults compared with the grains in (11.0) textured Co-alloy media

It should also be noted that in-plane circumferential anisotropy has not yet been achieved in (10.0) oriented media.

2.3.2 Preferred orientation

Whenever a crystalline material is deposited onto an amorphous substrate, a certain degree of preferred orientation (PO) is obtained (PO is also referred to as a crystallographic texture). The specific texture of the film depends mainly on the crystal structure and substrate-adatom interaction.

The driving force behind the PO is the minimization of the surface (interface) free energy either by developing the lowest energy planes at the film-substrate interface or by growing the lowest energy planes at the surface. The lowest energy planes vary with crystal structure. Based on single crystal growth observations [89], some of the known facets for crystals grown under equilibrium states are: a) (111) planes for fcc Cu, diamond, ZnS and CaF_2 structure; b) (110) planes for bcc metals and B2 (CsCl) structure. The latter can also develop (100) and (112) planes when the crystals grow larger; c) (100) planes for NaCl structure; d) (00.2), (10.0) and (10.1) planes for hcp structure.

Unlike the single crystals, which are grown close to equilibrium conditions with all the surfaces being free, the texture of deposited films is governed by both the surface and interface free energy. Therefore a crystallographic texture can develop either during the nucleation stage before nuclei impingement or during the growth stage after such impingement. Accordingly, the textures can be classified as either nucleation textures or growth textures.

The following are the textures that are usually developed in deposited films: Co-alloy films usually have the (00.2) texture for the hcp phase and the (111) texture for the fcc phase. MgO (NaCl structure) films usually develop the (200) texture [90], Cr (bcc) films usually have the (110) texture when grown at room temperature, and the (200) texture when grown at higher temperatures (250°C) [91-94]. NiAl (CsCl structure) develops either the (110) or the (112) texture [38].

Nucleation textures are formed during the initial stage of film deposition. When the deposition conditions enable the adatoms to have enough mobility on the substrate surface, the nuclei can more or less approach the equilibrium shape before they impinge with each other. The orientation of the nuclei depends on the relative values of the surface energy and interface energy. Such deposition conditions include:

1. The interaction between substrate and adatoms forming the nucleus is weak compared to the interaction amongst nucleus atoms.
2. The supersaturation is small.
3. The application of a substrate bias, which gives the adatoms extra kinematic energy from the bombardment of the sputtering gas and therefore emits loosely bonded atoms from the surface.
4. The sputtering gas pressure is low.
5. The nuclei must be large enough so that their surface can be described in terms of crystallographic planes.

In deposition processes, the supersaturation may be high in the chamber. The Ar pressure may also be high. To reduce the grain size, the substrate surface is sometimes modified to enhance the interaction between the substrate and adatoms. When these conditions are fulfilled, the nuclei are randomly oriented. In the growth stage after the impingement of nuclei, certain grains with lowest surface

energy will grow faster than others. The film will be gradually dominated by the grains with this favorable orientation. This kind of PO is called growth texture.

It was found [95] that the Cr (200) texture can be initiated directly on the substrate surface while the Cr (110) texture appears not to nucleate on the substrate surface, but rather to form as a result of growth. Fig. 2.6 shows that the PO of Cr films changes from (110) to (200) as the substrate temperature increases. This is because the development of texture changes from being dominated by growth to being dominated by nucleation.

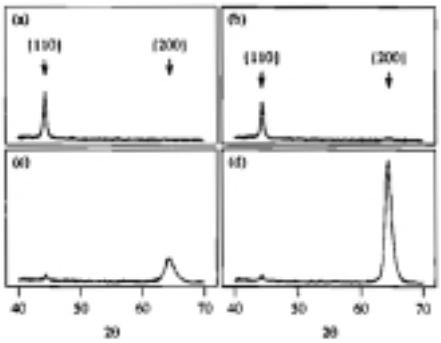

Fig. 2.6 (up) The X-ray diffraction patterns of Cr (175 nm)/Glass films deposited at a) 45°C, b) 105°C, c) 200°C, d) 260°C [69] (© 1990 IEEE).

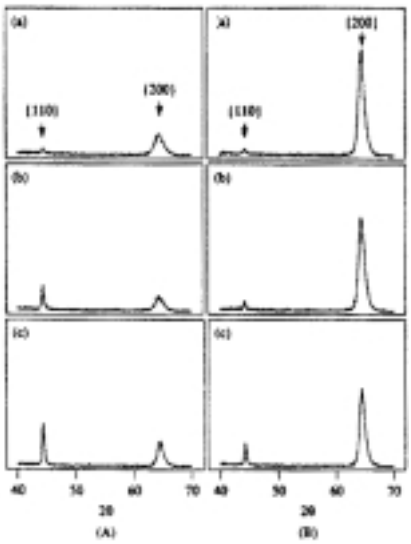

Fig. 2.7 (right) X-ray diffraction patterns of Cr/glass films of a) 170 nm, b) 250 nm c) 400 nm thickness at A) 200°C B) 260°C [69] (© 1990 IEEE).

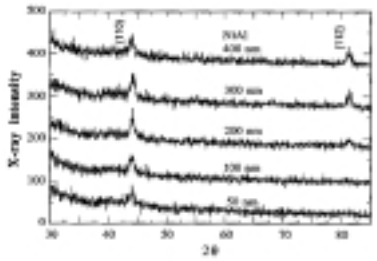

Fig. 2.8 NiAl films at varies thickness [98].

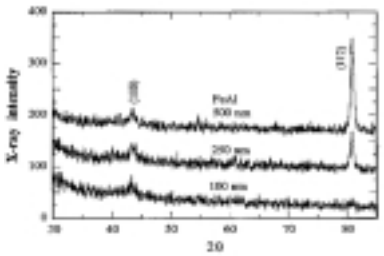

Fig. 2.9 FeAl films at varies thickness [98].

Fig. 2.10 (110) dark-field TEM image of a 400 nm thick NiAl film on glass substrate [39] (© 2000 IEEE, courtesy of Yu-nu Hsu).

At elevated substrate temperatures, the mobility of atoms is high, the nucleation rate is low, and the nuclei can reach the equilibrium shape before impingement. Because of the relative values of surface and interface free energy, the Cr nuclei tend to take (200) orientations. However, as can be seen in Fig. 2.6 and Fig. 2.7, some of (110) oriented grains remain in the film because the ideal equilibrium conditions are not perfectly realized during deposition. As the film grows thicker there will be a greater volume of (110) oriented grains because of their faster growth. The x-ray diffraction curves in Fig. 2.7 show an increase of (110) peak intensity and a corresponding decrease of the (200) peak intensity as the film thickness increases.

It is interesting to note that materials with the B2 structure [96] develop different textures than those with the bcc structure. NiAl [38] and FeAl [97] tend to have the (112) texture mixed with the (110) texture when they are deposited at room temperature. The (112) texture gets stronger as the film grows thicker, suggesting a growth texture (Fig. 2.8 and 2.9). Fig. 2.10 is a TEM cross-section dark-field image [39] of a 400-nm thick NiAl film, which shows that most of the (110) grains are near the film-substrate interface.

2.3.3 Degree of texture

To achieve a high degree of PO of the magnetic layer there are two main considerations. First, how to obtain a good texture of the underlayer; Second, how to obtain epitaxial growth of the magnetic layer on the underlayer.

2.3.3.1 Texture of underlayer

Many underlayer materials have been studied for the magnetic recording media, such as, β-W [99], Ti [100], Cr, Mo, W [101,102], Ga [103] Ni_xP [31,104], Cr/seedlayer (NiP_3, $TiSi_2$, C, CrSi, etc.) [105,106], Cr/CrNi [107], Cr/pre-coating (Cr, Ta, W and Zr) [108], NiCuP [109], Cr/amorphous carbon substrate [110], $Cr_{75}Ti_{25}$/CoTi (B2 structure) [111,112], Cr/NiAl [84], etc. Among these materials, CrX [113] and Cr/NiAl [4] are the most frequently used underlayers for longitudinal Co-alloy media.

To obtain a high degree of Cr (200) texture, the adatoms should have a high degree of surface mobility. A preferred way of doing this is through a heated substrate, where the T_{sub} is between 200°C and 300°C, and the Ar pressure is kept low [114]. By monitoring the texture quality using XRD rocking curves, Shan *et al.* [115] found that the degree of texture of both CrRu underlayers and CoCrPtTa magnetic layers improved monotonically as the substrate temperature increased.

Using a Ta seedlayer [108,116] can also improve Cr (200) texture. Ta serves as an excellent wetting layer and provides enough mobility for the Cr adatoms to nucleate in the (200) orientation.

Another way of obtaining Cr (200) textures is to deposit a seedlayer of MgO [90, 117]. Because of its NaCl structure, MgO thin films usually obtain the (200) texture when deposited at room temperature. In this approach, substrate preheating is avoided so that grain size of Cr layer and the subsequent Co-alloy layer can be well controlled.

To study the angular distribution of the PO in the layers of recording media, an electron diffraction method has been developed [118-120]. Although this method needs TEM sample preparation, which is destructive to the disk, it has several advantages over the XRD rocking curves. First, the amorphous layer and the Al substrate can be completely removed. These contribute to either a diffuse background intensity (Glass, NiP) or overlapping peaks (e.g. Al (200) overlaps with Cr (110)). Secondly, the electron diffraction technique allows the study of the crystallographic textures layer by layer. This is useful when the XRD peaks of the different layers overlap with each other, for example, MgO (200) and Cr (200), NiAl (112) and Cr (112), etc.

Using this method, Tang *et al*. [121] analyzed the degree of texture of MgO (200), Ta (110), Co-alloy (11.0)/Cr(200), and Co-alloy (10.1)/Cr (110). The authors found that the texture axis distribution angle α, which is comparable to the full width at half maximum (FWHM) of XRD rocking curve, to be 12°, 10°, 6°, 6°, respectively for these films. Using the same method, Lu *et al*. [85] analyzed the different layers of media CoCrPtTa/Cr/NiAl. They determined α to be about 14° for the NiAl layer, and 10° for both the Cr and CoCrPtTa layers. Not only did they find that the texture degree of the Co-alloy (10.0) is weaker than that of Co-alloy (11.0) and Co-alloy (10.1), but also that there are randomly oriented Co-alloy grains, which are seldom found in (11.0) oriented media.

A similar media Co-alloy/CrV/NiAl has been investigated by J. Li *et al*. for the 10Gbit/in2 areal density demonstration [4]. The results from a XRD pole figure also show a wide angular distribution (20°) of the (112) PO around the film normal. By using a CrV intermediate layer, the CrV(112) PO was more enhanced compared to the film with a Cr intermediate layer. Moreover, the magnetic layer was found to have fewer randomly oriented Co-alloy grains, which is due to the enhancement of the epitaxy through better lattice match.

Parker *et al*. [122] have found that CrV alloys have the effect of enhancing the (200) texture degree. The V content can be adjusted up to $Cr_{50}V_{50}$ because of the complete solubility of V in Cr. In their work 50 nm thick CrV films were sputter deposited onto NiP/Al-Mg substrates at 25±1°C with 50V bias. Electron diffraction patterns (EDPs) of the Cr film showed clearly that both (110) and (200) oriented grains exist in the underlayer, while the CrV EDP showed only a strong (200) texture. The XRD experiments in the same paper indicate that the Co-alloy layer has better epitaxy on a CrV underlayer than on a pure Cr underlayer. This brings up the second important consideration for obtaining a high degree of PO of the magnetic layer, namely the epitaxy between the underlayer and the magnetic layer.

2.3.3.2 Epitaxy

The lattice parameters of Co-alloys for magnetic recording are usually larger than those of pure Co because most of the alloying elements (e.g. Pt and Ta) have larger atomic radii than Co. Also, some of the atoms, such as B, are in interstitial sites, which also expand the lattice. It is critical to obtain lattice matching between the magnetic layer and the underlayer in order to obtain good epitaxial

growth, which in turn increases the degree of texture, reduces the interfacial stress and stacking fault density. On the other hand, if the lattice match gets too poor for epitaxy, the underlayer will be nonfunctional. For example, when Ta concentration becomes too large in the CoCrPtTa/Cr media many CoCrPtTa grains tend to orient with the (00.2) planes parallel to the film plane [123].

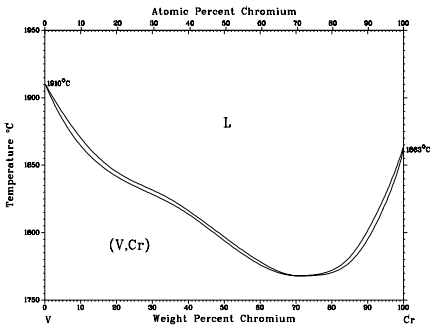

Fig. 2.11 Cr-V phase diagram [124]

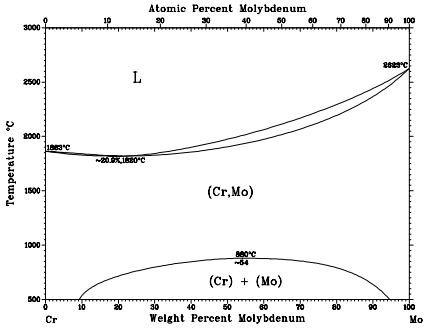

Fig. 2.12 Cr-Mo phase diagram [124]

Several CrX alloys have been tried to accomplish good lattice matching. Actually when one looks up the binary phase diagrams and lattice parameters, one finds that there are not many CrX alloys that are suitable for lattice matching with Co-alloys. CrMn, CrMo, CrOs, CrRu, CrSi, CrTc, CrTi, CrV, CrW are possible alloys. It appears that the CrV is the best in terms of solubility. The Cr-V phase diagram (Fig. 2.11) shows complete mutually solubility between V and Cr in the solid state. Since V has the same bcc structure as Cr, the lattice parameter of CrV underlayer can be adjusted continuously between Cr lattice parameter (0.2884 nm) and V lattice parameter (0.3027 nm).

In addition, alloys like CrMo (Fig. 2.12) and CrW whose equilibrium phase diagrams exhibit miscibility gaps may also be used because phase separation is unlikely to happen in deposited films. Moreover, since both W and Mo have large melting point, films of CrW and CrMo will form smaller grains. Most of the above mentioned alloys have been tried as underlayer materials. CrV[122], CrW [125], CrTi[126-128], CrRu [115], CrSi [127], CrMn [129] have all been investigated and have been found to improve the magnetic and recording properties of the media.

Vegard's law [130,131] is commonly used in calculating the lattice parameters of CrX alloys. The law postulates a linear dependence of lattice spacings with composition, but does not often hold over large composition ranges for metallic solid solutions. Nevertheless, within small composition ranges a linear extrapolation may be acceptable. Wong and Ying [132] have shown that the lattice parameter of CrV and CrMo alloys can be predicted using Vegurd's law. Lu *et al*. have shown the lattice parameter of CoCrPtTa with different Pt contents varies linearly within the composition range [133].

Lattice mismatch problems can be further alleviated by introducing an intermediate layer, which can either be a bcc CrX alloy or an hcp Co-alloy [134-138]. The values of the lattice parameters of the intermediate layer are chosen to be between that of underlayer and magnetic layer. Thus the mismatch can be

spread across two interfaces. Zhang *et al*. [139] also found that the media with an hcp non-magnetic intermediate layer, has better thermal stability as well as better recording properties.

In summary, Co-alloy magnetic films can have (10.1), (11.0), and (10.0) crystallographic textures when deposited onto CrX underlayers of (110), (200), (112) textures, respectively. The degree of the Co-alloy texture depends on the quality of the CrX texture and the extent of epitaxial growth. The underlayer texture depends on the CrX composition, the initial texture type, the interaction with the substrate, and processing parameters, while the quality of the epitaxy depends mainly on the chemical bond matching and the lattice matching between the magnetic layer and the underlayer.

2.4 Stacking faults and fcc phase

2.4.1 Introduction

The element Co has the hcp structure (space group $P6_3/mmc$) at room temperature and transforms to the fcc structure (space group $Fm\bar{3}m$) at 422°C [124]. This is unlike the elements Ti, Ru, Re, Zr, etc, which remain hcp until they melt. The hcp↔fcc transformation in Co is first order and therefore often occurs with superheating (hcp→fcc) or supercooling (fcc→hcp).

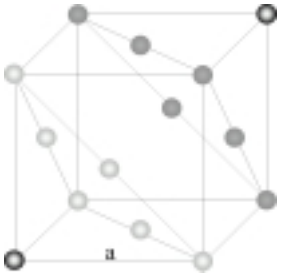

Fig. 2.13(a) Unit cell of the fcc structure.

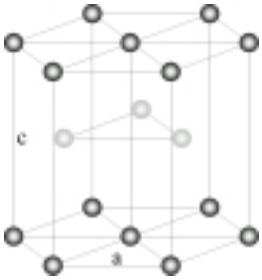

Fig. 2.13(c) Unit cell of the hcp structure.

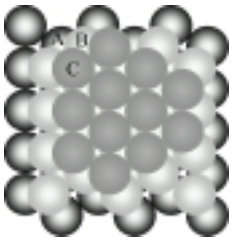

Fig. 2.13(b) Stacking of (111) planes.

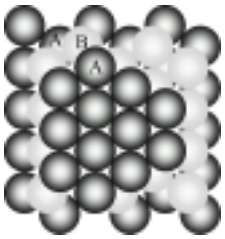

Fig. 2.13(d) Stacking of (00.2) planes.

The unit cells and the stacking sequence of hcp and fcc structure are shown in Fig. 2.13. It can be seen that the hcp structure is formed by stacking the close packed planes in the sequence ABABAB…, while the fcc structure is formed by stacking the close packed planes in the sequence ABCABCABC…, where the letters represent the position of the centers of the atoms of each plane, as shown in

the figure. Any error in the order of the stacking of the close packed planes is referred to as a stacking fault. A stacking fault (SF) in an hcp phase produce a thin slab of an fcc phase, for example AB<u>ABC</u>BCBCB..., where the underlined planes represent the fcc slab. SFs exist in all close packed structures though the energy of formation differs from one alloy to another. The SF energy is an intrinsic property of a material. For hcp alloys that transform to fcc at higher temperatures, the SF energy is lower than in those hcp alloys which do not transform to fcc [140].

Stacking faults (SFs) can be classified as either growth faults or deformation faults. A growth fault occurs by incorrect stacking during the growth of the hcp or fcc phase. A deformation fault is caused by a shearing of the close packed plane as a result of resolved shear stress. Such a stress could be due to a lattice mismatch at the interface or by the difference in thermal expansion coefficient between the layers. The SF density is closely related to the process temperature: the closer to the transformation temperature, the smaller is the energy difference between hcp and fcc and the greater the number of faults [141,142].

In Co alloys the transformation temperature, $T_{hcp\text{-}fcc}$ and $T_{fcc\text{-}hcp}$, varies with composition. Although it is difficult to study the phase transformation below 800^{o}C due to slow diffusion in the bulk alloy, some results [124] suggest the transformation temperatures increase with the addition of Ir (up to 30%), Os, Re, Rh (up to 20%), Ru, Ca, Mo, Si, and decrease with the addition of Al, Mn, Ni, Pd. This implies that the amount of fcc regions and SF density may vary with Co-alloy composition. Since the process of sputter deposition is far from equilibrium, the normal substrate temperature (T_{sub}) of 250^{o}C in producing of longitudinal media is well within the range of the fcc$\leftrightarrow$hcp phase transformation temperatures. Therefore a large amount of SFs and a large quantity of fcc grains are expected if the Co-alloy compositions and process parameters are not carefully selected.

Fcc grains are detrimental to magnetic recording because the Co fcc phase has a small magnetocrystalline anisotropy energy. Investigation of fcc grains in Co-alloy media can be dated back to 1982, when Coughlin *et al*. found that sputtering gas contamination might induce the formation of fcc grains in perpendicular CoCr thin films [143]. The existence of stacking faults in recording media was also discussed in the late 1980s [144]. SFs normally give rise to striation contrast in the TEM image of the Co-alloy grains. However, unlike the fcc phase, the effect of stacking faults on magnetic and recording properties has not been fully understood until recently. This is because of the complicated convolution of the effect of SF with other effects, such as, composition, grain size, chemical segregation, stress, etc. Next sections elucidate the effect of both fcc grains and SFs on the magnetic and recording properties of Co-alloy longitudinal media.

2.4.2 Fcc grains

The magnetic anisotropy energy of Co fcc phase is about one order of magnitude lower than that of the Co hcp phase [145]. Consequently, the presence of fcc grains can significantly lower the H_c of magnetic recording media and cause thermal instability problems. These problems get more severe in the region of the recording transitions, where the grains experience strong demagnetizing fields. A

micromagnetic simulation confirms that percolation within the written bits happens through the low coercivity grains. Fig. 2.14 shows a map of such a transition. It can be seen that the low coercivity grains (circles) cause the transition to be rougher, generating more transition noise [146,147].

Hcp and fcc Co-alloys have many planes with similar d-spacings. There are however a few unique ones, such as, $(200)_{fcc}$, $(10.0)_{hcp}$, $(10.1)_{hcp}$ and $(10.2)_{hcp}$. Therefore the (200) reflection is used in x-ray diffraction (XRD) or electron diffraction (ED) to estimate the amount of fcc grains inside hcp Co-alloy thin films [148,149]. High-resolution transmission electron microscopy (HRTEM) can also distinguish a fcc grain from the hcp matrix by directly imaging the atomic stacking sequence of the close packed planes [150].

Fig. 2.14. A map of micromagnetic simulation at the transition showing the percolation happens where there are a large number of low coercivity grains [146] (© 1998 IEEE, courtesy of R. W. Chantrell).

Many factors cause the existence of fcc grains in the magnetic layer. Processing temperature is one of the most important factors. When a CoCrTa film is deposited onto a substrate at temperatures greater than 250°C, the H_c of the magnetic layer decreases because more fcc grains are formed [151]. This indicates that at high temperatures the hcp phase transforms to fcc phase and that a substantial amount of fcc phase can be retained upon cooling to room temperature. The temperature effect gives rise to a temperature dilemma: the magnetic layer needs a higher temperature to obtain better Cr segregation to exchange de-couple the magnetic grains, but such high temperatures may increase the amount of fcc phase in the magnetic layer.

A second factor causing fcc grains to form is gas contamination. This has first been shown in studies of perpendicular media [143], where introducing nitrogen gas into the sputtering chamber dramatically increased the appearance of the fcc grains thereby lowering the H_c. An XRD scan showed that the (200) peak of fcc increased significantly while the (00.2) peak was reduced and was replaced by (10.0) and (10.1) peaks. This result shows that not only does the nitrogen induce the formation of the fcc phase but it also makes the grains orient more randomly.

Studies on the impurity gas effects in *longitudinal* media [152-154] also show that introduction of oxygen results in a drastic reduction of the coercivity of the films. The coercivity reduction due to nitrogen is moderate and the effect of air is intermediate between the effects of O_2 and N_2. A close investigation on the nitrogen gas effect reveals that magnetic and recording properties, such as, H_c, S*, SNR, deteriorate significantly for the $Co_{72}Cr_{16}Pt_{12}$ alloy as the base pressure (the chamber was initially flushed with N_2) is increased from 10^{-8} to 10^{-6} Torr. [149].

The authors confirmed by plan-view electron diffraction that a large amount of fcc grains were present when the base pressure was higher than 10^{-6} Torr.

The alloy composition is also a very important factor in controlling the amount of fcc phase in Co-alloy thin films. From Fig. 2.15 it can be seen that the fcc phase becomes stable at lower temperature as the Ni content increase. Ni is an example of an fcc stabilizing element, as is Pt.

Pt addition causes another dilemma in searching for the ideal composition for magnetic recording alloy. Pt has been found to increase H_c by enhancing the magnetocrystalline anisotropy of CoCr-alloy [155-157]. However, adding more Pt gives rise to a greater "fcc tendency" [158] of the alloy. Consequently, greater amounts of fcc grains, or fcc regions bounded by SFs, exist in high Pt CoCrPt-alloys. An H_c-Pt composition curve of CoCrPt alloy present a peak around 18% of Pt [156], though it is more appropriate to plot K_u versus Pt content.

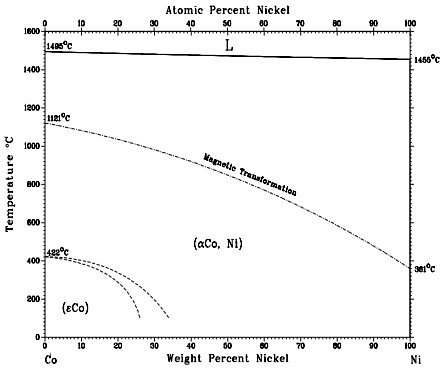

Fig. 2.15. Co-Ni phase diagram [124].

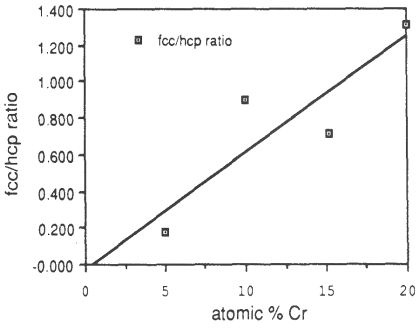

Fig. 2.16. Content of fcc phase in CoCr bulk alloys (reprinted from [160], © 1989, with permission from Elsevier Science).

The manifestation of the fcc tendency can also be found in the comparison of $Co_{84}Cr_{14}Ta_2$, $Co_{76}Cr_{12}Pt_{12}$, and $Co_{75}Ni_7Cr_6Pt_{12}$ thin films [159]. In Ref. [159] the authors reasoned that since in the $Co_{84}Cr_{14}Ta_2$ alloy the (00.2) lattice spacing matches almost exactly with the (110) spacing of Cr underlayer and that a 2% mismatch is found between $Co_{75}Ni_7Cr_6Pt_{12}$ and Cr, it is expected that more SFs and grains of fcc phase should be observed in the films of the latter composition. Consistently, $Co_{76}Cr_{12}Pt_{12}$, whose lattice match with Cr is in between the other two, shows an intermediate behavior. However, the phenomena can also be understood in terms of the greater amount of fcc stabilizing elements (Ni and Pt) in the CoNiCrPt alloy. Since there is such a large difference in the composition of the three alloys, the effect of composition on H_k, M_s and K_u of the Co-alloy should not be over looked.

The phase equilibria in the Co rich region of the Co-Cr phase diagram below 700°C have not been firmly established. This is due to sluggish diffusion in the temperature range. However, the work of Chan *et al*. [160] carefully studied the *bulk* Co-Cr alloy from 1.44% to 20% Cr. They find that the amount of fcc phase increases systematically with an increase in the Cr content (Fig. 2.16). Moreover, the SF density in the bulk materials was never found to be zero, no matter how the samples were heat-treated.

2.4.3 Stacking faults

Planar defects which appear as striations in TEM images have been observed for many years in plan-view TEM images of Co-alloy thin films [144,161-163]. These striations were determined to be stacking faults by electron nano-diffraction [164] and high-resolution TEM [20]. It was found that SFs exist all through the thickness of Co-alloy film [20], indicating that SFs occur even in the nucleation stage of the film growth.

Unlike the fcc phase, stacking faults show almost no trace in a regular θ–2θ XRD scans of Co-alloy media. According to Warren [165], SFs in a hcp system can cause streaking and hence peak broadening in all the diffraction spots along c-axis direction except the ones whose Miller indices satisfy h-k=3n, (n=0, 1,2,3…). Accordingly, among the low index reflections, (10.0), (10.1), (10.2), (10.3) will have streaks, (00.2), (11.0) will not have streaks.

There are several ways to detect SFs. XRD is the most quantitative way. However, in longitudinal media, the c-axis directions are in the film plane. As a result, all the peak broadening from the SF lies in the film plane. These broadenings cannot be observed by normal θ–2θ XRD scans, but an in-plane θ–2θ scan using glazing incident beam does reveal them [148]. Synchrotron radiation has to be used to obtain greater signal to noise ratios in such studies. Quantitative information of growth fault and deformation fault probabilities can be obtained by curve fitting the XRD spectra. Fig. 2.17 shows such XRD scans of two CoCrPt media grown at 10^{-6} and 10^{-5} Torr base pressures [149]. The fits to the experimental data are shown as solid lines. By curve fitting, the SF probabilities and total percentage of fcc-like region can be obtained. It was determined that the higher base pressure samples have more SFs and total fcc-like environment.

SF can also be detected by TEM imaging techniques, such as, diffraction contrast imaging [39,166] or high resolution imaging [166-168]. Since the atomic arrangement is clearly seen in HREM images, characteristics of the SFs can be easily determined [167]. By measuring the percentage of the faulted area of a high resolution image (Fig. 2.18), the SF density of that particular grain can be determined accurately. The value may be used to estimate the SF density of the whole sample.

Electron diffraction can also be used to study the SFs. Simply by taking plan-view electron diffraction patterns, one can determine qualitatively the SF densities [169]. Fig. 2.19 shows an electron diffraction pattern (EDP) of a (11.0) oriented Co-alloy media. The streaks from the (10.1), (10.2), and (10.3) reflections can be clearly observed. However, it should be noted when the film texture is (10.0), only rings like (00.2), (11.0), with h-k=3n are present in a plan-view image or EDP. Hence, there will not be either any streaks in the EDP or SF contrast in bright field or high-resolution images. This problem can be solved by tilting the TEM specimen to a higher angle [169,170]. A similar problem exists in the XRD setup. Sample tilting or asymmetric XRD scans should be used to measure the SF density in (10.0) textured Co-alloy thin films.

There are several causes for SFs in a Co-alloy thin film. Since the atomic arrangement inside a SF region is same as that of fcc phase, all the above mentioned causes of the fcc grains are also applicable for SFs. For example, it has

been found that high substrate temperature promotes the formation of SFs [171]. It has been found that the SF density increases with substrate temperature up to 260°C [167].

Fcc stabilizing elements, such as, Pt or Ni will also increase the SF density. The commonly sputtered Co films have a c/a ratio of less than the ideal close packing value of 1.633. The addition of the large Pt atoms causes the c/a ratio to approach that of the ideal value, which in turn makes it energetically easier for the crystallites to form with either an hcp stacking or fcc stacking.

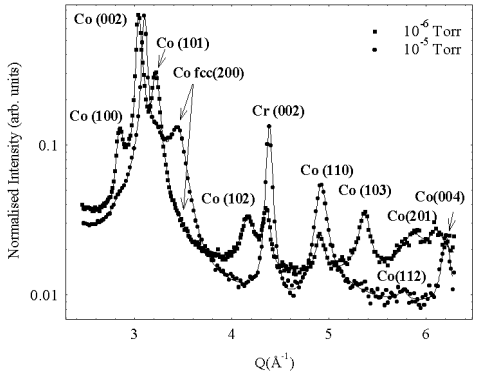

Fig. 2.17. In-plane θ–2θ scans of two CoCrPt media grown at 10^{-6} and 10^{-5} Torr. The fits to the experimental data are shown as solid lines [148] (courtesy of Helen Laidler).

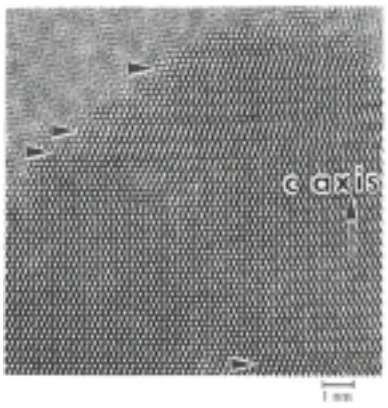

Fig. 2.18 High resolution TEM image showing SFs in a Co-alloy grain [168] (© 1996 IEEE).

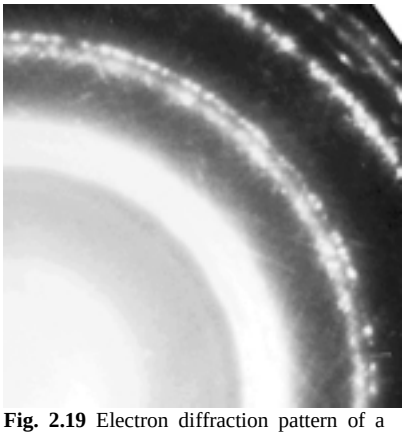

Fig. 2.19 Electron diffraction pattern of a CoCrPtTa film in (11.0) texture. The streaks are due to the SFs [169] (© 2000 IEEE).

Another important cause of SFs is stress. Stress may arise from the difference in the thermal expansion coefficients or lattice mismatch between the layers [159]. As determined by XRD [172] most of the SFs in the longitudinal media are deformation faults caused by stress. It has been demonstrated that $Co_{64}Cr_{22}Pt_{14}$ on Cr has a higher SF density than that of the media on $Cr_{82}Ta_{18}$. The latter film has better lattice match than the former. Moreover, the two samples have the same probability of producing growth faults; only the probability of deformation faults of the former is higher that the later. This strongly suggests that lattice mismatch between the magnetic and the underlayer plays an important role in controlling the

stacking fault density. Stress as an cause for SFs is also supported by high resolution TEM observations [173]. By comparing CoCrTa/Cr and CoCrPt/Cr thin films, it was found by high resolution TEM that increasing the Pt or Ta content increases the SF density. Since Pt and Ta have much larger atomic size than Co or Cr, the increase of Pt or Ta causes an expansion of the Co-alloy lattices. These results indicate that internal stress at Co-alloy/Cr interface causes SFs.

Both composition and lattice match affects the SF density, which in turn affects the magnetic properties of the Co-alloy media. However, composition directly affects the M_s and K_u of the film, while lattice match strongly affects epitaxy and the spread of texture orientation of the magnetic layer, which are both closely related to the magnetic properties [57, 122]. Therefore it is very difficult to discriminate the real effect of SFs on the magnetic and recording properties of Co-alloy media. Hence, it is not surprising that many research findings in the past contradict with each other.

For example, several groups [167,174,175] observed H_c increases with SF densities and improves media noise by promoting elemental segregation in the site of SFs due to Suzuki effect [176,177]. Later work did not find that SFs contribute to the improvement of magnetic performance [150,169]. The earlier findings may be due to multi-domain phenomena in the media, where Co-alloy grains could be as large as 50 nm. There is also a contradiction in the trend of SF density varying with substrate temperature [167,175]. This reflects the difficulty in estimating the SF density in Co-alloy thin films.

Recently the effect of SFs on magnetic properties and recording properties has been convincingly demonstrated [148,172,178]. The high SF density samples were shown to have more significant magnetic viscosity effects, which may cause significant thermal instability problems.

Moreover, research on the effect of the SF density in single crystal Co-alloy films has shown a strong correlation between SF density and magnetocrystalline anisotropy constant [170]. It was found that SF density negatively affects the anisotropy and the anisotropy temperature dependence.

2.5 Composition and segregation

2.5.1 Introduction

As the areal density in longitudinal recording approaches 100Gbits/in^2, there is a need for significant improvement of the intrinsic and extrinsic magnetic properties of the Co-alloys to achieve shorter transition lengths, low media noise, and higher thermally stability of thin film media. To make the recorded information thermally stable, a high value of the ratio of K_uV/k_BT is required [3,179,180]. Since V, the volume of magnetic grains, decreases with higher areal density, greater K_u materials are necessary for increasing the recording density.

Moreover, large H_c and low M_s values are essential for higher linear density and lower media noise [181]. It is also necessary to obtain intergranular magnetic separation to lower the exchange interaction [182]. The recent modeling of 100

Gbits/in^2 areal density [180] used media parameters of $K_u = 2.5\times10^6$ erg/cc, M_s = 300 emu/cc, while a recent laboratory demonstration of 30 Gbits/in^2 media used Co-alloy media with M_s of 320 emu/cc, K_u over 2.2×10^6 erg/cc and a remnant coercivity (H_{cr}) of 4900 Oe [183]. Obviously, more stringent control of the Co-alloy composition is necessary to achieve superior magnetic properties for higher density media. On the other hand, since element segregation is the best way of magnetically de-coupling the grains [184, 185] finding the right composition to enhance chemical segregation at the grain boundary is another mission for alloy improvement. This section covers both the effect of composition on the intrinsic magnetic properties and on chemical segregation within Co-alloy media.

2.5.2 Alloy composition

Pure Co has a M_s = 1400 emu/cc, K_u = 4.5 $\times10^6$ erg/cc, and a Curie temperature (T_c) of 1404 K. Many elements have been alloyed with Co in order to decrease M_s while keeping K_u relatively high,. Some of the alloy investigated for thin film media include: CoP [186], CoPt [187], CoNi [188], CoNiCr [189,190], CoCrTa [191], CoCrPr [192,193], CoCrPt [28,194,195], CoNiPt and CoNiPd [196]. High M_s values used to be needed to obtain high signal output for the reading was done by an inductive ring head. With the introduction of GMR heads (see Chapter 10) large M_s values are no longer necessary, which not only reduces magnetostatic coupling at the transitions by decreasing the $4\pi M_s/H_k$ value, but also inspires numerous studies of greater variety [197-200] of the Co-alloy with larger number of elements [201].

Throughout the 1990s, CoCrTa, CoCrPt and CoCrPtTa were the most popular alloys used by the hard disk industry. CoCrTa has very good noise properties, CoCrPt has high K_u, H_k and H_c, while CoCrPtTa is a compromise between the former two alloys. A large research effort has been devoted to understand the compositional dependence of the magnetic and recording properties as well as the microstructures of the thin films of Co-Cr-Pt-Ta systems.

The study of CoCrPtB alloys began in the early 1990s [202-205]. The coercivity of the CoCrPtB film was found to be very large and the noise level was low compared to other alloys of the same period of time. Therefore CoCrPtB has drawn increasing attention. Recently, CoCrPtB was also found to have a narrower grain size distribution and better intergranular de-coupling than the CoCrPtTa thin film [16,206]. Therefore, CoCrPtB is now being widely used at the beginning of the 21st century.

Research on the effect of Cr, Ta, and Pt on the magnetic properties of CoCrPtTa thin films has been extensively performed leading to a comprehensive understanding of the ternary/quaternary alloys. In 1993 Doerner *et al*. reported that increasing the Cr concentration in CoCrPt alloys results in an improved signal to noise ratio (SNR) [207]. The H_c of the CoCrPt film increased with higher Cr concentration. This is because of the Cr segregated toward grain boundaries causing better exchange de-coupling between the grains. A nearly linear decrease of M_s with increased Cr concentration has been demonstrated (Fig. 2.20). Doerner *et al.* also reported that an increase of Pt concentration has little effect on M_s, T_c

and SNR; however, the H_c increased effectively with higher Pt content. This is believed due to the large K_u of the alloy.

The effect of Pt was further investigated in the low concentration range ($(Co_{86}Cr_{12}Ta_2)_{100-x}Pt_x$, x=0-6%)[155] and high concentration range ($(Co_{83.6}Cr_{16.2})_{100-x}Pt_x$, x= 0, 13, 20, 40%)) [156]. It was found that adding Pt causes a linear M_s decrease (Fig. 2.21). The M_s decrease caused by Pt addition is nearly 8 times less than that caused by the Cr addition. The maximum H_c exists for Pt < 20%. The decrease of H_c with higher Pt additions is believed to be caused by a decrease in the epitaxy at the CoCrPt and Cr interface, and also by the presence of fcc phase.

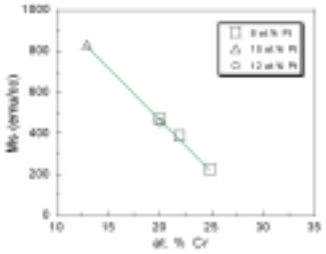

Fig. 2.20. M_s decrease in CoCrPt alloy due to Cr additions [207] (© 1993 IEEE).

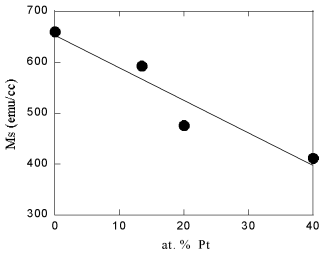

Fig. 2.21. M_s decrease in CoCrPt alloy due to Pt additions [156]

There are two main difficulties in the measurement of the intrinsic magnetic properties of Co-alloys from polycrystalline thin films. First, there is significant elemental segregation both within the grains [208] and to the grain boundaries [209]. It is very difficult to relate the measured magnetic properties to the nominal composition. For example, in the case of a $Co_{79}Cr_{16}Ta_6$ thin film, the maximum Cr concentration at the grain boundary is determined to be 23%, while inside the grains, the Cr concentration fluctuates between 8 and 11% [210]. In fact, the intrinsic magnetic properties of the polycrystalline films are dominated by the core magnetic grains because the grain boundaries are thought to be non-magnetic due to high Cr concentration. To further complicate matters, the degree of chemical segregation varies with the deposition conditions. Thus, different research groups often report incongruent results on same CoCr-alloy compositions.

The second difficulty comes from the small granular structure and the 2-d random orientation of the polycrystalline film. It is difficult to measure the K_u of such films accurately, since the precise demagnetization energy of the film cannot be estimated. Therefore, it is much better to determine compositional dependence of basic magnetic properties of CoCr-alloy using single crystal thin films. [55,58, 157,201,211-214]. The effect of Cr and Pt composition on the magnetic properties of CoCrPt, CoCrTa, and CoCrPtTa single crystalline films has been studied by Inaba *et al*. [58,201]. The Co-alloy thin films were deposited onto single crystal MgO (110) substrates with Cr or CrTi as underlayers to obtain a good lattice match. As a result, single crystal films with (10.0) orientation were obtained. Three series of Co-alloys which have been studied are: $Co_{96-x}Cr_xTa_4$ (x = 8-19%), $Co_{88-y}Cr_yPt_{12}$ (y = 15, 19%) and $(Co_{73}Cr_{15}Pt_{12})_{100-z}Ta_z$ (z = 0-5%).

It has been found that the absolute magnetization (M_{s0}) and Curie temperature (T_c) values decrease linearly (Fig. 2.22) with an increase Cr content in the Co_{96-}

$_xCr_xTa_4$ and $Co_{88-y}Cr_yPt_{12}$ systems and vanish at Cr concentrations of 33%. The magnetization at 285K vanishes when the Cr concentration reaches 27%. CoCrPt has a higher T_c and K_u than the CoCrTa films. For example, K_u of the $Co_{88}Cr_8Ta_4$ at 290K is 2.2×10^6 erg/cc, while K_u of $Co_{73}Cr_{15}Pt_{12}$ is about 3.7×10^6 erg/cc. Both M_s and K_u decrease with Ta additions, however as shown by Fig. 2.23, H_k remains constant up to 4 % Ta. Beyond this concentration, K_u and H_k values decrease abruptly. This clearly demonstrates that excess Ta additions to the CoCrPt system degrades the magnetic properties. As discussed above, the magnetic properties of polycrystalline films depend strongly on the Co-rich core grains due to the Cr segregation at the grain boundaries. It was shown that the temperature dependence of M_s and K_u for the $Co_{81}Cr_{15}Ta_4$ polycrystalline thin film is more like that of $Co_{88}Cr_8Ta_4$ single crystal film than that of $Co_{81}Cr_{15}Ta_4$ single crystal film [201].

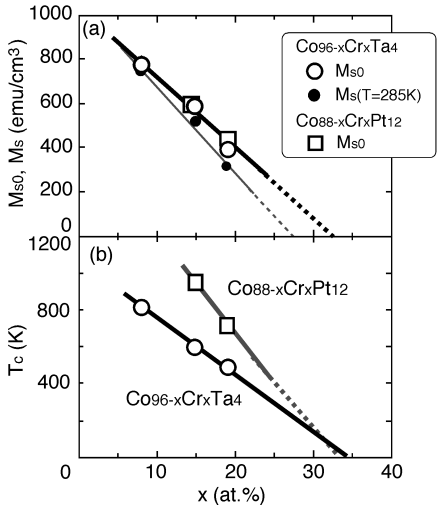

Fig. 2.22. M_s and T_c variation with Cr concentration [201] (© 2000 IEEE, courtesy of N. Inaba).

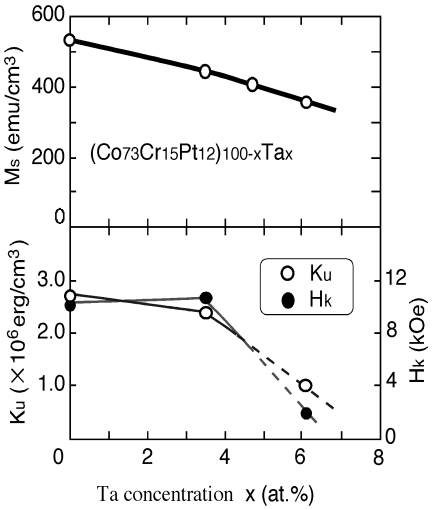

Fig. 2.23. M_s and K_u variation with Ta concentration [201] (© 2000 IEEE, courtesy of N. Inaba).

M_s and H_c of CoCrPtB thin film with B addition up to 15 %, Pt up to 20%, Cr up to 20% have been studied [202,203]. The dependence of M_s on Cr and Pt is similar to the case of CoCrPtTa media. M_s decreases linearly with B additions. A recent study [215] showed that the M_s decrease rate caused by adding B is similar to that caused by adding Pt. Moreover, it has also been showed that the H_k increase rate due to B addition is similar to that due to Pt addition. Magnetic force microscopy (MFM) studies [205] of the micromagnetic structure of CoCrPtB/Cr thin films have shown that CoCrPtB/Cr films have a smaller magnetic volume and lower magnetic roughness than CoCrPt/Cr media.

2.5.3 Chemical segregation

Experimental and modeling work have shown that exchange coupling between the grains of magnetic thin films is largely responsible for the media noise [216,217]. This intergranular coupling causes the formation of magnetic clusters,

which are much larger than the individual crystalline grains. Inside the magnetic clusters, the grains are crystallographically randomly oriented but all have the same magnetization direction. Consequently, the transition region between two opposite recorded bits has a zigzag like profile instead of a sharp continuous line [71,216,218-220]. This zigzag transition makes the transition center fluctuate randomly from transition to transition resulting in a timing jitter-induced noise. A detailed review of the relationship between media noise and intergranular coupling can be found in Ref. [221]. The key to making low-noise media is to minimize strong exchange interaction between the magnetic grains. Since the exchange coupling acts over short distance and the interaction decreases exponentially with the separation, magnetic separations as little as 1 nm might be sufficient to de-couple the neighboring grains.

There are generally three ways to de-couple the magnetic grains. One is to physically separate the grains, which can be achieved by using low mobility conditions during deposition of the underlayer and (or) magnetic layer. According to Thornton's model [222] discussed in section 2.2.3, voided films can be obtained under high Ar pressure and low substrate temperature with no bias [26-29,185]. Growing thicker columnar underlayers is also found to be effective in reducing media noise [30, 31]. Physical separation can also be achieved by using extremely low melting point alloys for the underlayer materials [103]. The physical separation method is not utilized for higher density recording media, due to its undesirable crystallographic texture, poor crystallinity, poor corrosion resistance and large surface roughness.

A second method of decoupling grains is to have non-magnetic phases, such as oxides, in the grain boundaries. In the past O_2 has been shown to reduce media noise by forming oxidized grain boundaries [223]. CoO or SiO_2 have been deposited together with Co-alloys resulting in a complete separation of the magnetic grains by the nonmagnetic materials [66,195,224,225]. However, films made by this kind of deposition tend to have a poor degree of crystallographic texture, poor corrosion resistance and a larger amount of the fcc phase.

The third way to achieve intergranular decoupling is through chemical segregation at the grain boundary. Processing conditions required for composition segregation in thin magnetic films are opposite to those used for physical segregation. High substrate temperatures, low sputter pressures, and bias, are used in combination to drive the segregation of one or more elements to the grain boundaries. These deposition conditions are congruent with what is required for other microstructural features, such as, epitaxial growth, control of stacking fault density and crystallographic texture. Therefore this method is considered the best way to magnetically separate the Co-alloy grains.

The phenomena of chemical segregation in Co-alloy thin films was reported as early as the 1960s, when thick grain boundaries were observed in CoP and CoNiP thin films [186,226-229]. The thickness of the separation was about 4nm. The grain boundaries were believed to be composed of phosphorous, which was later confirmed by X-ray energy dispersive analysis (EDAX) in a transmission electron microscope (TEM) investigation [230].

A large number of papers have been written on the studies of the chrysanthemum pattern (CP) phenomena [231]. Since this phenomena is mainly observed in very thick perpendicular films we will not discuss it in this review.

Precise determination of chemical segregation in CoCrPtTa thin films has been shown using Nano-probe EDAX and EFTEM since 1993 [184, 232-234]. These two methods have a spatial resolution of about 1-2 nm, which is about the same dimension as the width of the grain boundary [159]. The former can provide precise quantitative results while the latter also presents 2-D elemental mapping of the films.

Cr segregation. It has been unambiguously found that Cr segregates to the grain boundaries in CoCrTa, CoCrPt and CoCrPtTa thin films. Fig. 2.24 shows plan-view EFTEM images of $Co_{84}Cr_{12}Ta_4$/Cr media deposited at T_{sub}=250^{o}C. It can be clearly seen from the Cr composition maps that Cr is depleted within the grains (dark contrast) and that Cr is enriched in the grain boundary regions (bright contrast). Similar results were found in a cross-sectional TEM specimen. Results [81] from Nano-Probe EDAX from 29 grain boundaries showed that the normal grain boundaries have a Cr content from 19 to 34 % (mean 23% Cr), while bicrystal grain boundaries have a lower level of Cr (mean 17% Cr). The Cr composition in the Cr depleted regions was found to be less than 7%. The full width at half maximum (FWHM) of the composition profile across the grain boundaries is about 4 nm. More recently, Cr segregation has been demonstrated by Nano-Probe EDAX [210] that the thickness of the Cr-enriched shell is about 1nm in $Co_{81}Cr_{15}Ta_4$ alloy. This thickness is close to that observed by HRTEM [159], which shows $Co_{84}Cr_{14}Ta_2$ film has a 0.5 to 1 nm amorphous like grain boundaries.

It has also been discovered that more Cr segregates to the grain boundaries as substrate temperature (T_{sub}) increases [209]. The films will exhibit an increase in H_c with the increasing T_{sub} up to 250-300^{o}C, partly because of the decrease of exchange coupling by the Cr segregation. Further increases in T_{sub} will cause H_c to drop due to the formation of fcc phase. It has also been found that S* [235] and the ΔM peak [236], which are indicators of degree of exchange coupling, decreased with an increase of T_{sub}. In addition, an applied bias has a similar effect on the H_c, S* and ΔM peak as T_{sub} [237].

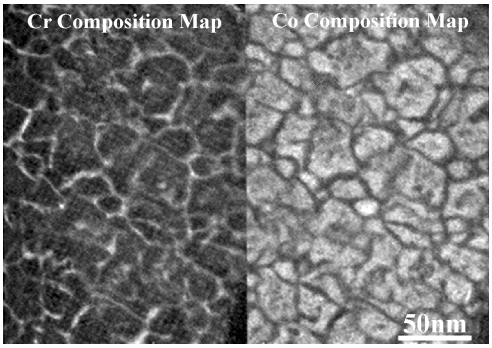

Fig. 2.24 Plan-view Cr and Co composition map of a CoCrTa thin film [81] (© 1998 IEEE, courtesy of J. E. Wittig).

Cr segregation in CoCrPt films has also been observed [232, 233], but the amount of Cr at the grain boundaries was found to be less than in the CoCrTa films. In the case of $Co_{74}Cr_{13}Pt_{13}$ (25 nm)/CrTi (50 nm) media deposited at T_{sub}=300^{o}C, the Cr concentration at grain boundaries was determined to be 16-18%, which is only 3-5 % greater than the overall Cr composition. This may well explain why HRTEM could not observe thick amorphous like grain boundaries in the CoCrPt media.

Cr segregation is also observed within the grains [234]. The segregation sites within the grains are most likely to be defects, especially *small angle boundaries* between two CoCrTa crystallites that nucleate separately on one Cr grain. Such defects are discussed in Ref. [237].

Type of grain boundary. Wittig *et al*. [81] found that Cr segregated more to the high angle grain boundaries than to the coherent (semi-coherent) 90^o bicrystal boundaries. They found the mean Cr concentration in high angle boundaries was found to be 23%, while the mean Cr concentration in bicrystal boundaries was 17%. Similar results have been reported by Inaba *et al*. [210], who found in $Co_{79}Cr_{15}Ta_6$ thin films that at high angle boundaries the maximum Cr concentration was 23% with the Cr-rich region thickness of about 1nm. At bicrystal boundaries the Cr composition was determined to be 18% and the width of the Cr enriched region was greater than 2 nm. These results suggest that the driving force of Cr segregation is stronger toward the high angle boundaries than toward the bicrystal boundaries.

Metal	high angle GBE (mJ/m^2)	coherent twin GBE (mJ/m^2)
Al	324	75
Cu	625	24
Ag	375	8
Au	378	15
Ni	866	43

Table 2.4. Grain boundary energy of high angle grain boundaries and coherent grain boundaries (reprinted from [140], © 1995, with permission from Elsevier Science).

This phenomenon can be understood by the fact that high angle grain boundaries have much larger grain boundary energy (GBE) than the bicrystal grain boundaries. Physically a non-coherent grain boundary has a more open structure, which better accommodates solute atoms than would a coherent grain boundary. Table 2.4 list GBE of selected elements.

Inter-layer diffusion. Interdiffusion between the $Co_{84}Cr_{12}Ta_4$ layer and Cr layer (T_{sub} = 250^{o}C) was not observed by EFTEM work [81,184]. On the other hand, magnetic measurements which are more sensitive than the structural analysis have found that M_s, S* and the ΔM peak decrease and H_c increases with an increase of T_{sub} in Co/Cr bilayers [238]. The use of a pure Co layer eliminated the possibility of intergranular segregation leaving only interlayer diffusion as the mechanism for Cr segregation. However, the magnetic properties varied only slightly when the T_{sub} was less than at 250^{o}C.

Interlayer diffusion can be enhanced by post-deposition annealing. Feng *et al*. [238] reported that after annealing at 550^{o}C for 1 hr. the M_s and S* of Co/Cr bilayer decreases by more than 30% and that the H_c increased from about 300 Oe to 800 Oe. In fact, interlayer diffusion is an effective way of transport of foreign

elements into grain boundaries of the CoCr-alloy films, in order to improve and tailor the magnetic properties of the media without destroying the structure or intrinsic magnetic properties of the core grains. Elements, such as, Mn [239,240], Zn [241], Cu [242] and C [243] have also been used to enhance the magnetic properties by interlayer diffusion.

Effect of Ta and Pt. It is very difficult to map the elements Ta and Pt using the EFTEM technique [208]. It has been found by EDAX that Ta and Pt are randomly distributed inside grains of both $Co_{81}Cr_{15}Ta_4$and $Co_{74}Cr_{13}Pt_{13}$ [184,233].

It has been widely accepted that Ta (not Pt) increases the segregation of Cr solute atoms to the grain boundaries. This is supported by magnetic measurements demonstrating that CoCrPtTa media with more Ta content exhibit lower S* and ΔM peaks and is also supported by elemental analysis indicating that Cr segregates more in CoCrTa films than in the CoCrPt films.

Inaba *et al.* [210] have used Nano-Probe EDAX to compare segregation in 5 CoCr-alloys (see Table 2.5). Thin films of the alloys were deposited under the same conditions as the CoCr-alloy (25nm)/ CrTi (50nm)/Si at 300^{o}C. Table 2.5 lists the measured Cr concentration at the grain boundaries and inside the grains as well as the average width of the Cr rich regions. The widths of the Cr rich region were determined as FWHM of the Cr distribution profile.

Table 2.5. Cr distribution in the CoCr-alloy films [210]

Alloy	Cr at GB	Cr inside grain	width
$Co_{81}Cr_{15}Ta_4$	25%	6-12 %	1 nm
$Co_{79}Cr_{15}Ta_6$	23%	8-11%	1 nm
$Co_{70}Cr_{14}Pt_{12}Ta_4$	18%	10%	2.3 nm
$Co_{73}Cr_{15}Pt_{12}$	18%	14%	2.2 nm
$Co_{79}Cr_{19}Pt_{12}$	24%		

It can be seen from the table that increasing the Ta concentration from 4 to 6% does not further enhance Cr segregation. However, more Ta was found at the grain boundaries. Comparing the first and third rows of the table, we notice that adding 12% Pt into the CoCrTa alloy decreases the Cr segregation. The increase of width indicates a smaller Cr concentration gradient from core to boundary, which implies that the Cr-rich phase at the grain boundaries may not be paramagnetic. As a result, the magnetic grains would not be effectively exchange de-coupled. Comparing the last two rows of the table, it can be seen that adding 4% Cr increases the Cr concentration at grain boundaries, which is 5% more than the overall composition. Considering that before the addition, it is only 3% more than the overall composition, it is reasonable to conclude that the addition of Cr still preferentially goes to the grain boundaries.

Boron diffusion. The Goldschmidt atomic radius of Boron atoms (0.097 nm) is much smaller than that of Co (0.125 nm), Cr (0.128 nm), Pt (0.138 nm) atoms. Therefore it is very likely that the B atoms can diffuse through interstitial sites as in the case of carbon diffusion [243], despite the fact that the close packed structure (hcp) does not have wide channels for interstitial diffusion compared with the body center cubic (bcc) systems. On the other hand the Cr atoms have to

diffuse by vacancy exchange, which is much slower than interstitial diffusion [244]. Nuhfer *et al.* [245] have shown that B segregates to the grain boundaries in CoCrPtB alloys. TEM and magnetic studies [16] has shown that adding 3-8% of boron causes a wider grain boundary phase and smaller S* and ΔM peak. These results indicate that better exchange de-coupled magnetic grains can be achieved by adding boron in the CoCrPt alloy.

Post-deposition annealing. Much effort has been devoted to post-deposition annealing of Co-alloy media [26, 115]. It has been demonstrated that post-deposition annealing can effectively magnetically de-couple the grains, providing excellent magnetic properties of the media. This is because annealing can take advantage of using high Pt compositions, which enhances the K_u of the CoCr-alloy media. At the same time, enough Cr can be driven to the grain boundary to exchange de-couple the grains. Without annealing, one has to add Ta and more Cr into CoCrPt to get better exchange de-coupling media, which in turn decreases K_u and H_k of the film.

For example, after rapid thermal annealing in vacuum, CoCrPt media can have an H_c as high as 6000 Oe and an M_rt = 0.3 memu/cc[247]. The H_c/H_k ratio is another way of monitoring the degree of coupling between the magnetic grains. This ratio has a maximum value of 0.5 for 2-D random media [246]. Mukai *et al*. [248] has shown that by depositing at lower temperatures and annealing at higher temperatures, the H_c of CoCrPt can be increased from 2000 to 4571 Oe and the H_c/H_k value increase from 0.2 to 0.46. Granular CoCrPt thin films were prepared by alternatively depositing $Co_{78}Cr_{10}Pt_{12}$ (2.5 nm) and SiO_2 (0.1-0.6 nm) layers onto a Cr underlayer on glass substrate at room temperature. The films were vacuum annealed up to 580^{o}C for 10 min. A large H_c increase from 2555 Oe to 5611 Oe and M_s drop from 701 emu/cc to 242 emu/cc was observed [249].

However, it should be noted that post-deposition annealing is not a cost-effective way for manufacturing of large quantities of disks. Seeking novel Co-alloy compositions is still the number one task to make high-density media with superior magnetic and recording properties.

2.6 Closure

We have shown that microstructural features such as grain size and distribution, preferred orientation, stacking faults, chemical segregation and composition of the media are all important in determining the magnetic properties and recording performance of longitudinal thin film media. Optimum media should have small grains with a narrow distribution, strong crystallographic texture with c-axis in plane, low stacking fault density and a high degree of chemical segregation to the grain boundaries.

Further research is important for the continuous improvement of these microstructural features. However, as the grain size gets smaller, the superparamagnetic limit will necessitate the use of high K_u materials [179] such as L1o-alloys or new media design such as AFC media [250,251].

Acknowledgements

We wish to thank our colleagues at Carnegie Mellon University and Seagate Technology for many helpful discussions. We especially thank Prof. David Lambeth for long term collaboration on thin film research. BL wishes to thank Dr. Dieter Weller for the constant support of the writing. He also wants to thank Ms. Marge Cain for organizing most of the references. DEL wishes to acknowledge the many students and postdoctorals that have worked with him and also the ongoing financial support of the Data Storage Systems Center at CMU under a grant ECD-8907068.

References

[1] Relation of Properties to Microstructure, American Society for Metals, Cleveland Ohio, (1954)
[2] Magnetic Properties of Metals and Alloys, American Society for Metals, Cleveland Ohio, (1959)
[3] S. H. Charap, P. -L. Lu, Y. He, IEEE Trans. Magn. **33**, 978 (1997)
[4] J. Li, M. Mirzamaani, X. Bian, M. Doerner, S. Duan, K. Tang, M. Toney, T. Arnoldussen, M. Madison, J. Appl. Phys. **85**, 4286 (1999)
[5] D. Weller, and A. Moser, IEEE Trans. Magn. **35**, 4423, (1999)
[6] E. T. Yen, S. Z. Wu, T. Thomson, R. Ristau, R. Ranjan, G. Rauch, IEEE Trans. Magn. **34**, 2730 (1999).
[7] T. P. Nolan, M. Hara, K Yoshida, M. Futamoto, J. Appl. Phys. **81**, 3922 (1997)
[8] H. Sato, J. Nakai, A. Kikuchi, H. Mitsuya, IEEE, Trans. Magn. **32**, 3596 (1996)
[9] A. KiKuchi, S. Kawakita, J. Nakai, T. Shimatsu and Mj. Takahashi, J. Appl. Phys. **79**, 5339 (1996)
[10] M. Lu, T. Min, Q. Chen, J. Judy, IEEE Trans. Magn. **28**, 3255 (1992)
[11] C. Gao, Z. S. Shan, R. Maimhall, Y. Liu, H. J. Richter, A. Barneu, G. C. Rauch, D. J. Sellmyer, J. Appl. Phys. **81**, 15 (1997)
[12] M. Takahashi, A. Kikuchi, H. Hara, H. Shoji, IEEE Trans. Magn, **34**, 1573 (1998)
[13] G. C. Rauch, C. Byun, E. R. C. Johns, and C. Messinger, J. Greggi, Jr., IEEE Trnas. Magn. **28**, 3105 (1992)
[14] Y. Takahashi, Y. Yajima, S. Kojima, Y. Hosoe, J. Appl. Phys. **87**, 5699 (2000)
[15] J. Soderlund, L.B. Kiss, G. A. Niklasson , C. G. Granqvist, Phys. Rev. Lett. **80,** 2386 (1998)
[16] Y. Kubota, L. Folks and E. E. Marinero, J. Appl. Phys. **84**, 6202 (1998)
[17] M. Doerner, K. Tang, T. Arnoldussen, H. Zeng, M. G. Toney, D. Weller, IEEE Trans. Magn. **36**, 43 (2000)
[18] J. P. Hirth and K, L. Moazed, *Physics of Thin films*, edited by G. Hass and R. Thum, Academic Press Inc., pp.97, (1967)
[19] J. J. K. Chang, Q. Chen, G. L. Chen, R. Sinclair, J. Appl. Phys. **81**, 3943 (1997)
[20] C. A. Ross, F. M. Ross, G. Bertero, K. Tang, IEEE Trans. Magn. **34**, 282 (1998)
[21] K. L. Chopra, *Thin Film Phenomena*, McGraw-Hill Book Company, pp142, (1969)
[22] R. W. Vook, Int. Metals Rev. **27**, 209 (1982)
[23] J. A. Thornton, Ann. Rev. Mater, Sci. **7**, 239 (1977)
[24] R. Messier, R. C. Ross, J. Appl. Phys. **53,** 6220 (1982)
[25] C. R. M. Grovenor, H. T. G. Hentzell, D.A. Smith, Acta Metall. **32**, 773 (1984)
[26] G. Choe, IEEE. Trans. Magn. **31**, 2809 (1995)
[27] R. Ranjan, J. A. Christner, D. P. Ravipati, IEEE Trans. Magn. **26**, 322 (1990)
[28] T. Yogi, C. Tsang, T. A. Nguyen, K. Ju, G. L. Gorman, G. Castillo, IEEE Trans. Magn. **26**, 2271 (1990)
[29] T. Yogi, T. A. Nguyen, S. E. Lambert, G. L. Gorman, G. Castillo, IEEE Trans. Magn. **26**, 1578

(1990)
[30] T. Yogi, G. L. Gorman, C. H. Hwang, M. A. Kakalec, S. E. Lambert, IEEE Trans. Magn. **24**, 2727 (1988)
[31] T. Yamashita, L. H. Chan, T. Fujiwara, T. Chen, IEEE. Trans. Magn. **27**, 4727 (1991)
[32] A. Mazor, D. J. Srolovitz, P. S. Hagan B. G. Bukiet, Phys. Rev. Lett. **60**, 424 (1988)
[33] C. V. Thompson, Mat. Res. Sco. Symp Proc. **343**, 3 (1994)
[34] S. Yoshimura, D.D.Djayaprawira, T. K. Kong, Y. Masuda, H. Shoji, M. Takahashi, IEEE Trans. Magn. **36**, 2363 (2000)
[35] Y. Matsuda, Y. Yahisa, K. Sakamoto, Y. Takahashi, A. Katou, Y. Hosoe, IEEE Trans. Magn. **35**, 2640 (1999)
[36] W. Xiong, H. L. Hoo, IEEE Trans. Magn. **34**, 1570 (1998)
[37] S. I. Pang, J. P. Wang, E. W. Soo, T. C. Chong, IEEE Trans. Magn. **36**, 2366 (2000)
[38] L.L. Lee, D. E. Laughlin, D. N. Lambeth, IEEE Trans. Magn. **30**, 3951 (1994)
[39] D. E. Laughlin, B. Lu, Y. N. Hsu, J. Zou, D. N. Lambeth, IEEE Trans. Magn. **36**, 48 (2000)
[40] M. Takahashi, A. Kikuchi S. Kawakita IEEE Trans. Magn. **33**, 2938 (1997)
[41] J. Nakai, A. Kikuchi, M. Kuwabara, T. Sakurai, T. Shimatsu, M. Takahashi, IEEE Trans. Magn. **31**, 2833 (1995)
[42] S. Yoshimura, D. D. Djayaprawira, T. K. Kong, Y. Masuda, H. Shoji, M. Takahashi, J. Appl. Phys. **87**, 6860 (2000)
[43] Y. Hosoe, T. Kanbe, K. Tanahashi, I. Tamai, S. Matsunuma and Y. Takahashi, IEEE Trans. Magn. **34**, 1528 (1998)
[44] T. Kanbe, I. Tamai, Y. Takahashi, K. Tanahashi, and A. Ishikawa, Y. Hosoe J. Appl. Phys. **85**, 4717 (1999)
[45] T. Kanbe, Y. Takahashi, K. Tanahashi, A. Ishikawa, Y. Hosoe, IEEE Trans. Magn. **35**, 2667 (1999)
[46] S. Sun, C. B. Murray, D. Weller, L. Folks, A. Moser, Science **287**, 1989 (2000)
[47] S. Sun, C. B. Murry, H. Doyle, Mat. Res. Soc. Symp. Proc. **577**, 385 (1999)
[48] N. Mahvan, A. M. Zeltser, D. N. Lambeth, D.E. Laughlin and M. H. Kryder, IEEE Trans. Magn. **26**, 2277 (1990)
[49] J. P. Lazzari, I. Melnich and D. Randet, IEEE Trans. Magn. **3**, 205 (1967)
[50] J. P. Lazzari, I. Melnich and D. Randet, IEEE Trans. Magn. **5,** 955 (1969)
[51] D. E. Laughlin, B. Cheong, Y. C. Feng, D. N. Lambeth, L. L. Lee, and B. Wong, Scripta Metall. Mater. **33,** 1525 (1995)
[52] H. Gong, W. Yang, M. Rao, D. E. Laughlin, D. N. Lambeth, IEEE Trans. Magn. **35**, 2676 (1999)
[53] W. Yang, D. N. Lambeth, L. Tang, D. E. Laughlin, J. Appl. Phys. **81**, 4370 (1997)
[54] Y. P. Deng, D. N. lambeth, D. E. Laughlin IEEE Trans. Magn. **28,** 3096 (1992)
[55] W. Yang, D. N. Lambeth, D. E. Laughlin, J. Appl. Phys. **85**, 4723 (1999)
[56] M. Futomoto, M. Suzuki, N. Inaba, A. Nakamura, Y. Honda, IEEE Trans. Magn. **30**, 3975 (1994)
[57] N. Inaba, A. Nakamura, T. Yamamoto, Y. Hosoe, and M. Futamoto, J. Appl. Phys. **79**, 5354 (1996)
[58] N. Inaba, M. Futamoto A. Nakamura, IEEE Trans. Magn. **34**, 1558 (1998)
[59] B. Y. Wong, D. E. Laughlin, D. N. Lambeth, IEEE Trans. Magn. **27**, 4733 (1991)
[60] J. Ding, J. Zhu, IEEE Trans. Magn. **30**, 3978 (1994)
[61] T. Min, J. Zhu, J. Appl. Phys. **75**, 6129 (1994); M. Mirzamaani, C. V. Jahnes, M. A. Russak, J. Appl. Phys. **69**, 5169 (1991); O. Kitakami, N. Kikuchi, S. Okamoto, Y. Shimada, K. Oikama, Y. Otani, K. Fukamichi, J. Magn. Magn. Mater. **202**, 305 (1999).
[62] D. N. Lambeth, W. Yang, H. Gong, D. E. Laughlin, B. Lu, L. L. Lee, J. Zou, P. S. Harlee, Mat. Res. Soc. Symp. Proc. **517**, 181 (1998)
[63] M. Futomoto, N. Inaba, A. Nakamura, Y. Honda, Acta Mater. **46**, 3777 (1998)
[64] D. E. Laughlin, B. Y. Wong, IEEE Trans. Magn. **27**, 4713 (1991)
[65] K. Hono, B. Wang, and D. E. Laughlin, J. Appl. Phys. **68**, 4734 (1990)
[66] A. Murayama, S. Kondoh, and Mj. Miyamura, J. Appl. Phys. **75,** 6147 (1994)
[67] H. J. Lee, J. Appl. Phys. **63**, 3269 (1988)
[68] J. K. Howard, R. Ahlert and G. Lim, J. Appl. Phys. **61**, 3834 (1987)
[69] S. L. Duan, J. O. Artman, B. Wong, and D.E. Laughlin, IEEE, Trans. Magn. **26**, 1587 (1990)
[70] M. Mirzamaani, C.V. Jahnes, and M. A. Russak, J. Appl. Phys. **69**, 5169 (1991)
[71] J. D. Daval and D. Randet, IEEE Trans. Magn. **6**, 768 (1970)

[72] K. E. Johnson, M. Mirzamaani, and M. F. Doerner, IEEE Trans. Magn. **31**, 2721 (1995)
[73] T. Hirose, H. Teranishi, M. Ohsawa, A. Ueda, O. Ishiwata, T. Ataka, K. Ozawa, S. Komiya, A. Iida, IEEE Trans. Magn. **33**, 2971 (1997)
[74] M. Mirzamaani, K. Johnson, D. Edmonson, P. Ivett, and M. Russak, J. Appl. Phys. **67**, 4695 (1990)
[75] A. Kawamoto, F. Hikami, J. Appl. Phys. **69**, 5151 (1991)
[76] T. P. Nolan, and R. Sinclair, R. Ranjan T. Yamashita, J. Appl. Phys. **73**, 5117 (1993)
[77] Y. Hosoe, Y. Yahisa, R. Tsuchiyama, A. Ishikawa, K. Yoshida, Y. Shiroishi, IEEE Trans. Magn. **31**, 2824, (1995)
[78] J. J. K. Chang, Q Peng, Q. Chen, Z. H. Lin, E. Yen, G. L. Chen, H. N. Bertram, R. Sinclair, IEEE Trans. Magn. **33**, 885 (1997)
[79] Q. Chen, J. J. K. Chang, G. L. Chen, R. Sinclair, IEEE Trans. Magn. **32**, 3599 (1996)
[80] Z. H. Lin, E. T. Yen, J. J. K. Chang, Q. Chen, M. C. Tang, G. L. Chen, J. Appl. Phys. **81,** 3946 (1997)
[81] J. E. Wittig, T. P. Nolan, C. A. Ross, M. E. Schabes, K. Tang, R. Sinclair, J. Bently, IEEE Trans. Magn. **34**, 1564 (1998)
[82] X. G. Ye, J. G. Zhu, IEEE Trans. Magn. **28**, 3087 (1992)
[83] Q. Peng, H. N. Bertram, N. Fussing, M. Doerner, M. Mirzamaani, D. Margulies, R. Sinclair, S. Lambert, IEEE Trans. Magn. **31**, 2821 (1995)
[84] L.-L. Lee, D. E. Laughlin, L. Fang and D. N. Lambeth, IEEE Trans. Magn. **31**, 2728 (1995)
[85] B. Lu, D. E. Laughlin, D. N. Lambeth, S. Z. Wu, R. Ranjan and G. C. Rauch, J. Appl. Phys. **85**, 4295 (1999)
[86] C. L. Fu and M. H. Yoo, Acta Metall. Mater., **40**, 703 (1992),
[87] Z. W. Lu, S. H. Wei and A. Zunger, Acta Metall. Mater. **40**, 2155 (1992)
[88] B. Lu, J. Zou, D. N. Lambeth and D. E. Laughlin, IEEE Trans. Magn. **36**, 2357 (2000)
[89] E. Bauer, *Single-Crystal Films*, Edited by M. H. Francombe and H. Sato, Pergamon Press, pp.64, (1964)
[90] L.L. Lee, B. K. Cheong, D.E. Laughlin, D.N. Lambeth, Appl. Phys. Lett. **67**, 3638 (1995)
[91] H. J. Lee, J. Appl. Phys. **57**, 4037 (1985)
[92] S. L. Duan, J. O. Artman, B. Wong, D. E. Laughlin, J. Appl. Phys. **67**, 4913 (1990)
[93] D. P. Ravipati, W.G. Haines, J. L. Dockendorf, J.Vac. Sci. Technol. **A5**, 1968 (1987)
[94] J. Pressesky, S. Y. Lee, S. L. Duan, D. Williams, J. Appl. Phys. **69**, 5163 (1991)
[95] Y. C. Feng, D. E. Laughlin, D. N. Lambeth, J. Appl. Phys. **76**, 7311 (1994)
[96] L. L. Lee, DE. Laughlin, D. N. Lambeth, US patent **5693426**, (1997)
[97] L. L. Lee, D. E. Laughlin, D. N. Lambeth, J. Appl. Phys. **81**, 4366 (1997)
[98] L. L. Lee, PhD Thesis, "Improving cobalt alloy thin film media through novel engineering of underlayers" Carnegie Mellon University, (1997)
[99] R. Ranjan, J. Appl. Phys. **67**, 4698 (1990)
[100] T. Kogure and S. Katayama, N. Ishii, J. Appl. Phys. **67**, 4701 (1990)
[101] H. Suzuki, N. Tsumita, M. Hayashi, Y. Shiroishi, Y. Matsuda, IEEE Trans. Magn. **26**, 2280 (1990)
[102] J. K. Howard, J. Appl. Phys. **63**, 3263 (1987)
[103] M. Mirzamaani, C. V. Jahnes, M. A. Russak, IEEE Trans. Magn. **28**, 3090 (1992)
[104] R. Ranjan, J. Chang, T. Yamashita, and T. Chen, J. Appl. Phys, **73**, 5542 (1993)
[105] X. Tang, B. Reed, R. Zubeck, IEEE Trans. Magn. **30**, 3963 (1994)
[106] S. Duan, B. Zhang, C. Gao, G. C. Rauch, J. L. Pressesky, A. Schwartz, IEEE Trans. Magn. **30**, 3966 (1994)
[107] Y. Okumuram, M. Yashi, T. Akita, M. Maeda, X. B. Yang, H. Fujimori, IEEE Tran. Magn. **33**, 2974 (1997)
[108] H. Kataoka, T. Kanbe and H. Kashiwase, E. Fjita, Y. Yahisa K. Furusawa, IEEE, Tans. Magn. **31**, 2734 (1995)
[109] Y. Onishi, H. Matsumura, T. Hase, H. Hayashi, M. Sato K. Katsumoto, IEEE, Trans. Magn. **25**, 3887 (1989)
[110] M. Kuwabara, M. Sato Y. Onishi, M. R. Visokay, H. Hayashi H. Inoue, K. Muramatsu, J. Appl. Phys. **73**, 6686 (1992)
[111] T. D. Lee, IEEE Trans. Magn. **35**, 2628 (1999)
[112] S. Y. Hong, T. D. Lee, K. H. Shin, J. Appl. Phys. **85**, 4298 (1999)
[113] K. Sato, Y. Yoshida, M. Yamagishi, H. Ueno, H. Akimoto, E. N. Abarra, H. Kanai, Y. Uehara, I. Okamoto, Y. Yematsu, IEEE Trans. Magn. **35**, 2655 (1999)

[114] T. Kawanabe, J.G. Park and M. Naoe, Mat. Res. Soc. Symp. Proc. **232**, 21 (1991)
[115] Z. S. Shan, C. P. Luo, M. Azarisooreh. K. Honardoost, M. Russak, Y. Liu, J. P. Liu, D. J. Sellmyer, IEEE Trans. Magn. **35**, 2643 (1999)
[116] M. Mirzamaani, X. Bian, M.F. Doerner, J. Li, M. Parker, IEEE Trans. Magn. **34**, 1588 (1998)
[117] L. L. Lee, D. E. Laughlin, D. N. Lambeth, J. Appl. Phys. **79**, 4902 (1996)
[118] L. Tang and D. E. Laughlin, J. Appl. Crystal, **29**, 411 (1996)
[119] B. Lu, L. Tang, D. N. Lambeth, and D. E. Laughlin, "Grain Growth in Polycrystalline Materials", Proceedings of 3rd International Conference on Grain Growth, 529 (1998)
[120] L. Tang, S. Duan, D. E. Laughlin, Mat. Res. Soc. Symp. **562**, 105 (1999)
[121] L. Tang, Y. C. Feng, L. L. Lee, D. E. Laughlin, J. Appl. Crystal, **29**, 411 (1996)
[122] M. A. Parker, J. K. Howard, R. Ahlert and K. R. Coffey, J. Appl. Phys. **73**, 5560 (1993)
[123] K. Sin, J. M. Sivertsen, J. H. Judy, IEEE Trans. Magn. **30**, 4008 (1994)
[124] T. B. Massalski, Binary Alloy Phase Diagrams, 2nd edition, ASM International.
[125] S. Malhorta, D. Strafford, B. Lal, C. Gao, M. Russak, J. Appl. Phys. **85**, 6157 (1999)
[126] Y. Shiroishi, Y. Hosoe, A. Ishikawa, Y. Sugita, H. Suzuki, T. Ohno, M. Ohura, J. Appl. Phys. **73**, 5569 (1993)
[127] G. Choe, J. Appl. Phys. **79**, 4923 (1996)
[128] Y. Matsuda, Y. Yashi, J. Inagaki, E. Fujita, A. Ishikawa, J. Appl. Phys. **79**, 5351 (1996)
[129] L. L. Lee, D. E. Laughlin, D.N. Lambeth, IEEE Trans. Magn. **34**, 1561 (1998)
[130] L. Vegard, Z. Physik, **5**, 17 (1921)
[131] L. Vegard, Z. Krist. **67**, 239 (1928)
[132] B. Y. Wong, J. F. Ying, IEEE Trans. Magn. **35**, 2646 (1999)
[133] B. Lu, D. N. Lambeth, and D. E. Laughlin, S. D.Harkness, W. A. Lewis, Proc. Mater. Res. Soc., **562**, 117 (1999)
[134] M. Fotomoto, F. Kugiya, M. Suzuki, H. Takano. Y. Matsuda IEEE Trans. Magn. **27**, 5280 (1991)
[135] L. Fang, D. N. Lambeth, Appl. Phys. Lett. **65**, 3137 (1994)
[136] B. Zhang, W. R. Bennett, C. Gao. G. C. Rauch, IEEE Trans. Magn. **32**, 3590 (1996)
[137] J. Zou, D. E. Laughlin, D. N. Lambeth, IEEE Trans. Magn. **34**, 1582 (1998)
[138] K. Tanahashi, I. Tamai, S. Matsunuma, T. Kanbe, A. Ishikawa, J. Appl. Phys. **87**, 6857 (2000)
[139] L. Zhang, B. B. Lal, M. A. Russak, IEEE Trans. Magn. **35**, 2649 (1999)
[140] F. J. Humphreys and M. Hatherly, Recrystallization and Related Annealing Phenomena, p.69 Pergamon 1995
[141] T. Ericsson, Acta Metall. **14**, 853 (1966)
[142] T. C. Tisone, Acta Metall. **21**, 229 (1973)
[143] T. M. Coughlin, E. R. Wuori, J. H. Judy, J. Vac. Sci. Tech. **20**, 171 (1982)
[144] J. W. Lee, B. G. Demczyk, K. R. Mountfield and D. E. Laughlin, J. Appl. Phys. **61**, 3813 (1987)
[145] W. Sucksmith and J. E. Thompson, Proc. R. Soc. **A225**, 362 (1954)
[146] K. O Grady, N. S. Walmsley, C. F. Wood, R. W. Chantrell, IEEE Trans. Magn. **34**, 1579 (1998)
[147] N. S. Walmsley and R. W. Chantrell, J. Appl. Phys. **85**, 6154 (1999)
[148] L. Holloway, H. Laidler, J. Appl. Phys. **87**, 5690 (2000)
[149] C. Gao, S. Wu, J-P Chen, R. Malmhall, C. Habermeier, R. Sinclair, H. Laidler, K. O'Grady, IEEE Trans. Magn. **34**, 1576 (1998)
[150] S. E. McKinlay, N. Fussing, R. Sinclair, Mary Doerner, IEEE Trans. Magn. **32**, 3587 (1996)
[151] Y. Shen, B.Y. Wong and D.E. Laughlin, J. Appl. Phys. **76**, 8167 (1994)
[152] D. J. Mapps, N. Mahvan, M. A. Akhter, IEEE Trans. Magn. **23**, 2473 (1987)
[153] J. A. Thompson, D. A. Stevenson, IEEE Trans. Magn. **21**, 1441 (1985)
[154] S. Iwasaki, K. Ouchi, K. Saiki, M. Kimura, IEEE Trans. Magn. **22**, 1158 (1986)
[155] K. Utsumi, T. Inase, A. Kondo, J. Appl. Phys. **73**, 6680 (1993)
[156] P. Glijer, J. M. Sivertsen, J. Judy, J. Appl. Phys. **73**, 5563 (1993)
[157] O. Kitakami, N. Kikuchi, S. Okamoto, Y. Shimada, K. Oikama, Y. Otani, K. Fukamichi, J. Magn. Magn. Mater. **202**, 305 (1999).
[158] H. Yamaguchi M. Yanagisawa, IEEE Trans. Magn. **22**, 576 (1986)
[159] T. P. Nolan, R. Sinclair, R. Ranjan, T. Yamashita, J. Appl. Phys. **73**, 5566 (1993)
[160] L. H. Chan, G. Thomas, J. S. Gau, J. Magn. Magn. Mater. **79**, 95 (1989).
[161] J. W. Lee, B. G. Demczyk, K. R. Mountfield, and D. E. Laughlin, J. Appl. Phys. **63**, 2905 (1988)
[162] B. G. Demczyk, and D. E. Laughlin, Mater. Res. Soc. Symp. Proc. **119**, 158 (1988)

[163] J. W. Lee, K. R. Mountfield, and D. E. Laughlin, J. Appl. Phys. **63**, 3266 (1988)
[164] K. Hono. B. G. Demczyk, D. E. Laughlin, Appl. Phys. Lett. **55**, 229 (1989)
[165] B. E. Warren, *X-ray diffraction*, Dover Publications INC, pp. 298, (1969)
[166] T. P. Nolan, R. Sinclair, R. Ranjan, T. Yamashita, IEEE Trans. Magn. **29**, 292 (1993)
[167] B. Y. Wong, Y. Shen, D. E. Laughlin, J. Appl. Phys. **73**, 418 (1993)
[168] A. Ishikawa, and R. Sinclair IEEE Trans. Magn. **32**, 3605 (1996)
[169] B. Lu, J. Zou, D. N. Lambeth, D. E. Laughlin, Intemag 2000, #BP-04
[170] B. Bian, W. Yang, D. N. Lambeth, D. E. Laughlin, The 8th Joint MMM-Intermag Conference, #HA-03, 2001
[171] Y. Shen, B. Y. Wong, and D. E. Laughlin, J. Appl. Phys. **76**, 8174 (1994)
[172] P. Dova, H. Laidler, K. O'Grady, M. F. Toney, M. F. Doerner, J. Appl. Phys. **85**, 2775 (1999)
[173] R. Sinclair T. P. Nolan, G. A. Bertero, M. R. Visokay, Mat. Res. Soc. Symp. Proc. **313**, 705 (1990)
[174] L. Tang G. Thomas, M. R. Khan, S. L. Duan, N. Heiman, J. Appl. Phys. **69**, 5166 (1991)
[175] R. Ranjan, W. R. Bennett, G. J. Tarnopolsky, T. Yamashita, T. Nolan, R. Sinclair, J. Appl. Phys. **75**, 6144 (1994)
[176] R. Herschitz and D. N. Seidman, Acta Metall. **33**, 1547 (1985)
[177] H. Suzuki, J. Phys. Soc. Jpn. **17**, 322 (1962)
[178] G. J. Parker, B. Lu, T. J. Klemmer and R. W. Chantrell, The 8th Joint MMM-Intermag Conference, #HF-02, 2001
[179] D. Weller, A. Moser, L. Folks, M. E. Best, W. Lee, M. F. Toney, M. Schwickert, J. U. Thiele, M. F. Doerner, IEEE Trans. Magn. **36**, 10 (2000)
[180] H. N. Bertram, H. Zhou, R. Gustafson, IEEE Trans. Magn. **34**, 1845 (1998)
[181] K. E. Johnson, K J. Schulz, J. M. Severson, IEEE Trans. Magn. **29**, 3670 (1993)
[182] J. G. Zhu, H. N. Bertram, J. Appl. Phys. **63**, 3248 (1988)
[183] M. F. Doerner, X. Bian, K. Tang, M. F. Tony, K. Rubin, D. Weller, A. Moser, M. Mirzamaani, A. Polcyn, T. Minvielle,K. Takano, R. White, #GA-01, Intermag 2000
[184] M. Futamoto, N. Inaba, Y. Hirayama, K. Ito, Y. Honda, Mat. Res. Soc. Symp. Pros. **517**, 243 (1998)
[185] K. E. Johnson, J. B. Mahlke, K. J. Schulz, A. C. Wall, IEEE Trans. Magn. **29**, 215 (1993)
[186] T. Chen, D. A. Rogowski, R. M. White, J. Appl. Phys. **49**, 1816 (1978)
[187] M. Yanagisawa, N. Shiota, H. Yamaguchi, Y. Suganuma, IEEE Trans. Mag. **19**, 1638, (1983)
[188] H. Maeda, J. Appl. Phys. **53,** 3735, (1982)
[189] T. Yamada, N. Tani, M. Ishikawa, Y. Ota. K. Nakamura, A. Itoh, IEEE Trans. Magn. **21**, 1429 (1985)
[190] M. Ishikawa, N. Tani, T. Yamada, Y. Ota, K. Nakamura, A. Itoh, IEEE Trans. Magn. **22**, 573, (1986)
[191] R. D. Fisher, J. C. Allan, J. L. Pressesky, IEEE Trans. Magn. **22**, 352 (1986),
[192] T. Suzuki, N. Yoshida, U. Hwang, Y. Uchiyama, K. Ishibashi, J. Appl. Phys. **63**, 2929 (1988)
[193] M. R. Khan, R. D. Fisher, Neil Heiman, IEEE Trans. Magn. **26**, 118 (1990)
[194] I. L. Sanders, T. Yogi, J. K. Howard, S. E. Lambert, G. L. Gorman, C. Hwang, IEEE Trans. Magn. **25**, 3869 (1990)
[195] T. Shimizu, Y. Ikeda, S. Takayama, IEEE Trans. Magn. **28**, 3102 (1992)
[196] T. Inase, A. Kondo, J. Appl. Phys. **69**, 5160 (1991)
[197] H. Akimoto, I. Okamoto, M. Shinohara, IEEE Trans. Magn. **34**, 1597 (1998)
[198] T. Miyamoto, J. Nakai, H. Matsumura, K. Yoshikawa, M. Kuwabara, M. Visokay, H. Saffari, IEEE Trans. Magn. **31**, 2839 (1995)
[199] S. Yoshimura, D. D. Djayaprawira, H. Shoji, M. Takahashi, J. Appl. Phys. **87**, 6866 (2000)
[200] M. Takahashi, H. Shoji, S. Kadowaki, D.D. Djayaprawira, Y. Komori H. Domon, Appl. Phys. Lett. **76**, 3457 (2000)
[201] N. Inaba, Y. Uesaka, M. Futamoto, IEEE Trans. Magn. **36**, 54 (2000)
[202] N. Tani, T. Takahashi, M. Hashimoto, M. Ishikawa, Y. Ota, K. Nakamura, IEEE Trans. Magn. **27**, 4736 (1991)
[203] C. R. Paik, I. Suzuki, N. Tani, M. Ishikawa, Y. Ota, K. Nakamura, IEEE Trans. Magn. **28**, 3084 (1992)
[204] Y. Murakami, T. Yamamoto, A. Okabe, T. Yanada, K. Hayashi, K. Aso, J. Appl. Phys. **73**, 6674 (1993)
[205] P. Glijer, J. M. Sivertsen, J. H. Judy. IEEE Trans. Magn. **31**, 2842 (1995)
[206] G. R. Jones, K. O'Grady, X. Bian, M. Mirzamaani M. F. Doerner, #BP06, Intermag 2000

[207] M. F. Doerner, T. Yogi, D. S. Parker, S. Lambert, B. Hermsmeier, O. C. Allegranza, IEEE Trans. Magn. **29**, 3667 (1993)
[208] J. Bentley, J. E. Wittig, T. P. Nolan, Mat. Res. Soc. Symp. Pros, **517**, 205 (1998)
[209] Y. Yahisa, K. Kimoto, K. Usami, Y. Matsuda, J. Inagaki, K. Furusawa, S. Narishige, IEEE Trans. Magn. **31**, 2836 (1995)
[210] N. Inaba, M. Futamoto, J. Appl. Phys. **87**, 6863 (2000)
[211] A. Nakamura, M. Futamoto, Jpn. J. Appl. Phys. **32**, L1410 (1993)
[212] A. Nakamura, M. Kouguchi, M. Futamoto, Jpn. J. Appl. Phys. **34**, 2307 (1993)
[213] N. Inaba, Y. Uesaka, A. Nakamura, M. Futamoto, Y. Sugita, S. Narishige, IEEE Trans. Magn. **33**, 2989 (1997)
[214] W. Yang, D. N. Lambeth, D. E. Laughlin, J. Appl. Phys. **87**, 6884 (2000)
[215] R. Ranjan, H. J. Richter, J. Chen, S. D. Harkness, S. Z. Wu, R. Ristau, Er. Girt, C. Chang, R. M. Brochie, G. C. Rauch, S. Gangopadhyay, K. Subramanian, #HA-01, the 8th Joint MMM-Intermag Conference, 2001.
[216] T. Chen, IEEE Trans. Magn. **17**, 1181 (1981)
[217] J. G. Zhu, H. N. Bertram, IEEE Trans. Magn. **24**, 2706 (1988)
[218] J. N. Chapman, J. Phys. D **17**, 623 (1984)
[219] T. Chen, G. B. Charlan, J. Appl. Phys. **50**, 4285 (1979)
[220] D. D. Dressler, J. J. Judy, IEEE Trans. Magn. **Mag-10**, 674 (1974)
[221] J. H. Judy, IEEE Trans. Magn. **29**, 209 (1993)
[222] J. A. Thornton, J. Vac, Sci. Tech. **A4**, 3059 (1986)
[223] J. K. Howard, R. G. Simmons T. Yogi, US Patent No. **5066552** (1991)
[224] A. Murayama, M. Miyamura, S. Kondoh, J. Appl. Phys. **76**, 5361 (1994)
[225] R. Ranjan, M. Lu, T. Yamashita, T. Chen, IEEE. Trans. Magn. **30**, 3942 (1994)
[226] J. S. Judge, J. R. Morrison, D. E. Speliotis, J. Electronchem. Soc. **113**, 547 (1966)
[227] M. G. Miksic, R. Travieso, A. Arcus, R. H. Wright, J. Electrochem. Soc. **113**, 360 (1966)
[228] J. S. Judge, J. R. Morrison, D. E. Speliotis, J. Appl. Phys. **36**, 948 (1965)
[229] M. Aspland, G. A. Jones, B. K. Middleton, IEEE Trans. Magn. **Mag-5**, 314 (1969)
[230] K. Hono, D. E. Laughlin, J. Magn. Magn. Mater. **80**, L137 (1989)
[231] Y. Maeda, D. J. Rogers, O. Song, K. Takei, T. Ohkubo. S. Hirono, J. Suzuki, Y. Morii, IEEE Trans. Magn. **33**, 879 (1997)
[232] M. R. Kim, S. Guruswamy, K. E. Johnson, IEEE Trans. Magn. **29**, 3673 (1993),
[233] N. Inaba, T. Yamamoto, Y. Hosoe, M. Futamoto J. Magn. Magn. Mats. **168**, 222 (1997)
[234] J. E. Wittig, T. P. Nolan, R. Sinclair, J. Bentley, Mat. Res. Soc. Symp. Pros, **517**, 211 (1998)
[235] B. R. Natarajan, E. S. Murdock, IEEE Trans. Magn. **24**, 2724 (1988)
[236] P. I. Mayo, K. O'Grady, P. E. Kelly, J. Cambridge, I. L. Sanders, T. Yogi, R. W. Chantrell, J. Appl. Phys. **69**, 4733 (1991)
[237] B. Y. Wong, Y. Shen, D. E. Laughlin, J. Appl. Phys. **73**, 418 (1993)
[238] Y. C. Feng, D. E. Laughlin, D. N. Lambeth, IEEE Trans. Magn. **30**, 3948 (1994)
[239] J. Zou, B. Lu, T. Leonhardt, D. E. Laughlin, D. N. Lambeth, J. Appl. Phys. **87**, 6869 (2000)
[240] J. Zou, B. Lu, D. E. Laughlin, D. N. Lambeth, IEEE. Trans. Magn. **35**, 2661 (1999)
[241] J. Zou, PhD Thesis "Improvement of Co-Alloy Magnetic Media via Grain Boundary Diffusion and Intermediate Layers" Carnegie Mellon University, 2000
[242] W. Peng, Z. Qian, C. Yang, J. M. Sivertson, J. H. Judy, J. Appl. Phys. **85**, 4702 (1999)
[243] J. J. K. Chang, K. E. Johnson, H. Kawayoshi, P. Ling, M. Strathman, IEEE Trans. Magn. **34**, 1567 (1998)
[244] D. A. Porter, K. E. Esterling, Phase Transformations in Metals and Alloys. Van Nostrand Reinhold Company, 1980
[245] T. Nuhfer, T. F. Fliervoet, Y. N. Hsu, M. Doerner, D. E. Laughlin, unpublished research
[246] M. Sato, Y. Onishi, A. Nakaue, IEEE. Trans. Magn. **29**, 3685 (1993)
[247] J. P. Wang, L. P. Tan, M. L. Yan, T. C. Chong, J Appl. Phys. **87**, 6352 (2000)
[248] R. Mukai, K. Yamanaka, M. Oshiki. J. Appl. Phys. **81**, 3931, (1997)
[249] Y. Xu, J. P. Wang, Y. Su, J. Appl. Phys. **87**, 6971 (2000)
[250] E. N. Abarra, I. Okamoto, Y. Mizoshita, #AA-06, Intermag 2000
[251] M. Madison, T. Arnoldussen, M. Pinarbasi, M. Parker, M. Doerner, X. Bian, K. Tang. M. Mirzamaani, S. Yuan, J. Li, L. Lauchlan, L. Ingall, J. Raniseski, P. Fang, D. Margulies, E. Marinero, K. Rubin, K. Takano, E. Fullerton, D. Weller, A. Moser, M. E. Best, #HT-01, Intermag 2000